T.R.

GAZİANTEP UNIVERSITY

GRADUATE SCHOOL OF HEALTH SCIENCE

ANATOMICAL INVESTIGATION OF SAFE TRAJECTORY DETERMINING FACTORS IN ROBOTIC COCHLEAR IMPLANT SURGERY WITH COMPUTED TOMOGRAPHY IMAGES

Saliha Seda ADANIR

Ph.D. THESIS

DEPARTMENT OF ANATOMY

Anatomy PhD Program

SUPERVISOR

Prof. Dr. Piraye KERVANCIOĞLU

II. SUPERVISOR

Prof. Dr. Vedat TOPSAKAL

Gaziantep

2024

T.R.

GAZİANTEP UNIVERSITY

GRADUATE SCHOOL OF HEALTH SCIENCE

ANATOMICAL INVESTIGATION OF SAFE TRAJECTORY DETERMINING FACTORS IN ROBOTIC COCHLEAR IMPLANT SURGERY WITH COMPUTED TOMOGRAPHY IMAGES

Saliha Seda ADANIR

Ph.D. THESIS

DEPARTMENT OF ANATOMY

Anatomy PhD Program

SUPERVISOR

Prof. Dr. Piraye KERVANCIOĞLU

II. SUPERVISOR

Prof. Dr. Vedat TOPSAKAL

Gaziantep

2024

T.R.
GAZİANTEP UNIVERSITY
GRADUATE SCHOOL OF HEALTH SCIENCE
DEPARTMENT OF ANATOMY
Anatomy PhD Program

ANATOMICAL INVESTIGATION OF SAFE TRAJECTORY DETERMINING FACTORS IN ROBOTIC COCHLEAR IMPLANT SURGERY WITH COMPUTED TOMOGRAPHY IMAGES

Saliha Seda ADANIR

Thesis Defense Date : 12/01/2024

Approval of the Graduate School of Health Sciences

Assoc. Prof. Dr. Davut Sinan KAPLAN
Director of Graduate School of Health Sciences

I certify that this thesis satisfies all the requirements as a thesis for the degree of Doctor of Philosophy.

Prof. Dr. Piraye KERVANCIOĞLU
Head of Department of Anatomy

I certify that this thesis satisfies all the requirements as a thesis for the degree of Doctor of Philosophy.

Prof. Dr. Piraye KERVANCIOĞLU
Supervisor

Prof. Dr. Vedat TOPSAKAL
II. Supervisor

This thesis has been read and accepted, in scope and quality, as a thesis for the degree of Doctor of Philosophy.

Examining Committee Members	Signature
Prof. Dr. Piraye KERVANCIOĞLU	
Prof. Dr. Salih Murat AKKIN	
Prof. Dr. Belgin ALAŞEHİRLİ	
Assoc. Prof. Dr. İlhan BAHŞİ	
Assoc. Prof. Dr. Begümhan TURHAN	

DECLERATION

I hereby declare that all information in this document has been obtained and presented in accordance with academic rules and ethical conduct. I also declare that, as required by these rules and conduct, I have fully cited and referenced all material and results that are not original to this work.

January, 2024

Saliha Seda ADANIR

ACKNOWLEDGMENTS

I extend my profound gratitude to my esteemed thesis supervisor, Prof. Dr. Piraye KERVANCIOĞLU, who provided me with scientific support at every stage of my thesis and postgraduate education, supported and motivated me in every aspect.

I would also like to express my gratitude to my second thesis supervisor, Prof. Dr. Vedat TOPSAKAL, for his scientific contributions to my thesis.

Special thanks are due to Assoc. Prof. Dr. Ömer Faruk CİHAN for his support and contributions to my education throughout my postgraduate education.

I acknowledge the invaluable contributions of the faculty members of the Department of Anatomy at Gaziantep University, Faculty of Medicine, namely Prof. Dr. Mustafa ORHAN, Prof. Dr. Erdem GÜMÜŞBURUN, Assoc. Prof. Dr. İlhan BAHŞİ, and Assoc. Prof. Dr. Orhan BEGER, who have supported and enriched my education.

I am grateful to Student of Gaziantep University Faculty of Medicine, Intern Doctor Rabia Hafsa Yeşilyurt for the anatomical drawings she made for my thesis.

I am grateful to my esteemed colleagues with whom I have collaborated in our department.

I extend my appreciation to the research assistants and audiologists of the Ear Nose Throat Department at UZ Brussel Hospital for their assistance and camaraderie during my time there.

I would like to express my gratitude to the Scientific and Technological Research Council of Turkey (TÜBİTAK) for the support I received under the 2211-A Domestic PhD Scholarship Program during the first four years of my PhD education.

Finally, heartfelt thanks to my mother, who raised me and enabled me to reach the present day, always providing strength with her unwavering belief in me throughout this challenging process, my father, who I always felt by my side with his love and support, and sister Eda, my first friend and supporter in life

Infinite thanks…

TABLE OF CONTENTS

LIST OF ABBREVATIONS

BTA	Basal turn angle
BTL	Basal turn length
CAA	Cochlea apical angle
CBCT	Cone-beam computed tomography
CDL	Cochlear duct length
CH	Cochlea height
ChT	Chorda tympani
CI	Cochlear implant
CL	Cochlear length
CS	Conventional surgery
CT	Computed tomography
Ct	Canonus type
CW	Cochlear width
DFNM	Depth of the facial nerve mastoid segment
FN	Facial nerve
FNM	Facial nerve mastoid segment
FR	Facial recess
FRA	Facial recess angle
FRW	Facial recess width

HRCT	High resolution computed tomography
LC	Length of canonus
MPTA	Mastoidectomy and posterior tympanotomy approach
SNHL	Sensorineural hearing loss
RW	Round window
RWSI	Supero-inferior distance of round window
RWAP	Antero-posterior distance of round window
ST	Scala tympani
TC	Thickness of canonus

LIST OF FIGURES

LIST OF TABLES

ABSTRACT

ANATOMICAL INVESTIGATION OF SAFE TRAJECTORY DETERMINING FACTORS IN ROBOTIC COCHLEAR IMPLANT SURGERY WITH COMPUTED TOMOGRAPHY IMAGES

Saliha Seda ADANIR
Ph.D. Thesis, Department of Anatomy
Supervisor: Prof. Dr. Piraye KERVANCIOĞLU
II. Supervisor: Prof. Dr. Vedat TOPSAKAL
January 2024, 95 pages

The ideal trajectory to insert a cochlear implant array is defined by an entrance through the round window membrane and continues as long as possible parallel to the basal turn of the cochlea. Facial recess width and angle, canonus thickness, round window sizes, and cochlear orientation are important for determining the safe trajectory in both robot-assisted and conventional cochlear implantation surgery. In addition, it is thought that there may be a significant relationship between the postoperative electrode insertion depth degree and cochlear orientation. Here in this, thesis we examined the keyhole drilling trajectories of cochlear implantation surgeries performed with the HEARO Procedure to compare the critical anatomical structures between easy and difficult cases.

Preoperative and postoperative computed tomography images of patients who underwent robot-assisted and conventional cochlear implant surgery at UZ Brussel Hospital were included in the study. Radiological images in DICOM format were transferred to a dedicated software for analyses. OTOPLAN, (CASCINATION AG, Bern, Switzerland) was used for 3D reconstruction of the temporal bone, auditory ossicles, facial nerve, chorda tympani, cochlea, and round window. In addition, depth of the facial nerve, facial recess angle, and cochlear orientation angles were measured with RadiAnt DICOM Viewer. Facial recess width, facial recess angle, and distance between the facial nerve and safe trajectory were statistically smaller in patient whose safe distance to the facial nerve could not be guaranteed with intraoperative imaging. A significant positive correlation existed between basal turn angle and in-plane angle.

The facial recess anatomy was the most critical factor for safe robotic inner ear access in our series here. Additionally, insight on the cochlear orientation before robotic surgery helps ensure a collision-free trajectory and feasible (safer) approach angles to the cochlea. In both robotic and conventional surgery, preoperative assessment of cochlear dimensions is crucial for appropriate electrode selection and, consequently, for postoperative audiological outcomes. The findings of this study are considered to be a reference for future studies in achieving collision-free trajectory planning in robotic-assisted cochlear implant surgery.

Key words: Cochlea, Cochlear implantation, Facial recess, Robot-assisted cochlear implant surgery, Sensorineural hearing loss

ÖZET

ROBOTİK KOKLEAR İMPLANT CERRAHİSİNDE GÜVENLİ YÖRÜNGE BELİRLEYİCİ FAKTÖRLERİN BİLGİSAYARLI TOMOGRAFİ GÖRÜNTÜLERİNDE ANATOMİK İNCELENMESİ

Saliha Seda ADANIR
Doktora tezi, Anatomi Anabilim Dalı
Tez danışmanı: Prof. Dr. Piraye KERVANCIOĞLU
II. Tez danışmanı: Prof. Dr. Vedat TOPSAKAL
Ocak 2024, 95 sayfa

Cochlear implant cerrahisinde, elektrot dizisini yerleştirmek için ideal cerrahi yörünge, membrana tympani secundaria'dan geçen bir hatla tanımlanır ve cochlea'nın bazal dönüşüne mümkün olduğunca paralel olarak devam eder. N. facialis ve chorda tympani arasındaki açıklık olarak bilinen facial recess boyutları ve facial recess açısı, canonus kalınlığı, fenestra cochlea boyutları ve cochlea'nın basis cranii'deki oryantasyonu hem robotik hem de konvansiyonel cochlear implant cerrahisinde güvenli cerrahi yörüngeyi belirlemek için önemlidir. Bu çalışmada, kolay ve zor vakalar arasındaki bu anatomik yapıların karşılaştırılması ve bu yapıların güvenli cerrahi yörünge üzerindeki etkilerinin incelenmesi amaçlanmıştır.

Çalışmaya UZ Brussel Hastanesinde robot-yardımlı ve konvansiyonel cochlear implantasyon cerrahisi geçiren hastaların ameliyat öncesi ve ameliyat sonrası bilgisayarlı tomografi görüntüleri dahil edildi. DICOM formatındaki görüntüler analizler için özel bir yazılıma aktarıldı. Os temporale, ossicula auditus, n. facialis, chorda tympani, cochlea ve fenestra cochlea'nın 3 boyutlu rekonstrüksiyonu için OTOPLAN (CASCINATION AG, Bern, İsviçre) kullanıldı. Ayrıca RadiAnt DICOM Viewer ile n. facialis derinliği, facial recess açısı ve cochlear oryantasyon açıları ölçüldü. N. facialis'e güvenli mesafenin intraoperatif görüntüleme ile garanti edilemediği hastada facial recess genişliği, facial recess açısı ve n. facialis ile güvenli yörünge arasındaki mesafe istatistiksel olarak önemli derecede daha küçüktü. Cochlea'nın bazal dönüş açısı ile cerrahi yörünge açıları arasında anlamlı bir pozitif korelasyon mevcuttu.

Mevcut çalışmada güvenli robotik iç kulak erişimi için facial recess anatomisinin en kritik faktör olduğu görüldü. Ek olarak, robotik cerrahi öncesinde cochlear oryantasyona ilişkin bilginin, çarpışmadan uzak bir yörüngenin ve cochlea'ya uygun (daha güvenli) yaklaşma açılarının sağlanmasına yardımcı olabileceği saptandı. Hem robotik hem de konvansiyonel cerrahide, cochlea boyutlarının preoperatif değerlendirmesi, uygun elektrot seçimi ve dolayısıyla postoperatif odyolojik sonuçlar açısından çok önemlidir. Bu çalışmanın bulgularının, robot-yardımlı cochlear implantasyon cerrahisinde çarpışmasız yörünge planlamasının sağlanmasında gelecekteki çalışmalara referans olabileceği düşünülmektedir.

Anahtar kelimeler: Cochlea, Cochlear implantasyon, Facial recess, Robot yardımlı cochlear implantasyon cerrahisi, Sensörinöral işitme kaybı

1. INTRODUCTION AND AIM

Sensorineural hearing loss (SNHL) is a hearing deficit for the patient and a severe social burden with sociocultural consequences (1). Cochlear implants (CI) are currently state-of-the-art rehabilitation for patients with severe SNHL and allow daily verbal communication to compensate for the social burden of deafness (2). In deaf born children it will enable them to develop speech and language (1). The auditory pathways' tonotopic orientation and the brain's plasticity to adapt to another strategy for hearing have made a cochlear implant the most successful bio prothesis in medicine (3, 4). Roughly 65,000 CI surgeries are performed worldwide each year, and there are about 1 million CI users already (5, 6). CI surgery is a microsurgical procedure involving tasks performed on a submillimeter scale, necessitating accurate visual and tactile feedback (5, 7). The electrode array of CI is inserted into the cochlea, the lead array is put within the surgically drilled mastoid cavity, connecting to the stimulator receiver part that is surgically positioned beneath the skin of temporal region above and behind the pinna (8). In most cases of SNHL, the cause is at the cellular level in the inner ear and the anatomical structures of the internal ear are intact. Therefore, inserted electrodes can benefit from this architecture design for tonotopicity of the cochlea (9).

The mastoidectomy and posterior tympanotomy approach (MPTA) is accepted as the gold standard for access to the cochlea in cochlear implantation surgery however it still has a very small risk of facial nerve injury (<1%) (10). The least invasive entry to the internal ear is considered to be best through the round window and the golden standard for surgical approach via the facial recess has become the posterior tympanotomy combined with an atticoantor mastoidectomy. In the MPTA, a high-speed drill is used to gain access through the space called as facial recess (FR) between facial nerve mastoid segment (FNM) and chorda tympani (ChT) (7, 11). The special localization of the facial nerve (FN) within the temporal bone makes it vulnerable to trauma (12). Iatrogenic FN injury is one of the most severe complications of cochlear implantation surgery. Therefore, FN function is monitored electrophysiological during cochlear implantation surgery along with other otologic procedures (13, 14). Knowing anatomical relations of the facial nerve mastoid segment (FNM), FR sizes and the angle between the chorda tympani and facial nerve (FRA) is essential to avoid FN and ChT injuries during the CI surgery. HEARO is the world's first robotic surgical system for high precision, minimally invasive cochlear implantation (15). The robot and navigation-assisted keyhole surgery defined by the HEARO procedure have by protocol risk mitigation not to drill closer than 0.4 mm to the FN, while surgeons with conventional surgery can safely expose the FN from its bony canal called facial canal (3). Once the tympanic cavity has been accessed, access to the cochlea occurs through cochleostomy or the round window (RW) to insert the electrode array. The RW size and shape reported in the literature are well variable and most often not even round (16, 17). If the RW anatomy is suitable, insertion from the RW is thought to be the least traumatic approach (14). The secondary tympanic membrane covers the RW (15). During access to the cochlea via the round window, this membrane must be pierced (14, 16). Canonus is defined as a bony eminence that partially envelops and protects the RW. In robotic surgery, this structure is only drilled open as large as necessary (canonostomy) to pass the electrode array to insert through the round window. With conventional surgery, the canonus is completely removed (canonectomy) to allow the surgeon to estimate the direction of insertion whereas in robotic image guided surgery already warrants the right insertion angle. It is essential to estimate the canonus thickness before the surgery to plan this step meticulously in a way that its most structure and residual hearing preserving (3, 16-18).

With the development of surgical technologies, robotic systems have started to take place in various interventions in many fields, especially in urology, gynecology and neurosurgery. Current robot technology expands the surgeon's toolkit and allows for the execution of human-like tasks with superior accuracy, consistency and, stability in speed (5). Otology is thought to be an ideal field that can benefit from robots, given the rigid bone of the temporal bone for navigation and the necessity of precision in small operation areas. Over the past decade, the stake has been raised in using robotics for cochlear implantation (18). In addition, the main advantage of robotic surgery in otology is working on hard materials. On the other hand, otologic surgery demands high accurateness for the safety of the FN and small sizes in the internal ear. Robotic- assisted cochlear implantation surgery allows the surgeon to gain access to the internal ear in the most standardized way (3). Through robotic cochlear implantation, access to internal ear is achieved by image-guided minimally invasive tunnel drilling to electrode insertion into the cochlea (5, 19, 20).

The ideal trajectory to place a cochlear implant array is described by an entrance through the RW membrane and continues as long as possible parallel to the cochlear basal turn. It is generally accepted that the least invasive of most minor traumatic insertion will have to be in line with the basal turn and most preferably with alignment with the centerline of the scala tympani (ST). Today's electrodes still have some rigidity for the surgeon to be able to insert them deeper into cochlear spaces. This rigidity may also damage the wall of the cochlea (21). Cochlear implantation traumas including spiral ligament penetration bony spiral lamina fractures, basilar membrane rupture, and electrode array translocation into scala media and vestibuli have been reported (22-25). To account for such trauma, it is very significant to correctly determine the ideal and safe trajectory before surgery and to provide the patient with the suitable trajectory angle (10, 26).

The cochlear orientation is probably the most essential parameter for the calculation of the ideal surgical trajectory. It is reported that there are significant variations in cochlear orientation within the reference range. The orientation of the cochlea within the base of the skull is determined by the angle between its long axis and midsagittal axis (27). Another important parameter is for cochlear implantation is the variable anatomy of the cochlea, which is of key importance for implantation (28). It has been reported that cochlear diameter and width have a significant relationship with the electrode insertion depth degree (29). There have been studies reporting better auditory performance when implant arrays are correctly and to the highest accuracy well placed (29-32). Surgeons should pay attention to cochlear duct length (CDL) to have complete or maximum cochlear coverage by implant arrays. In addition, manufacturers already provide different lengths of arrays apart from the cochlear duct length anatomical landmarks such as the diameter of the RW membrane and dimensions of ST are subject of study to improve implant design and performance. So that safe surgical access to the cochlea, trauma to electrode insertion, and preservation of residual hearing are closely related to cochlear dimensions and cochlear orientation (28, 29, 33).

Facial recess sizes and angle, canonus thickness indeed, round window sizes and cochlear orientation are important for determining the safe trajectory in both robotic and conventional surgery. In addition, it is thought that there may be a significant relationship between the postoperative electrode insertion depth degree and cochlear orientation.

In this thesis, it is aimed to anatomically examine the surgical trajectories of cochlear implantation surgeries performed with the HEARO Procedure, to compare the critical anatomical structures between easy and difficult cases, and to investigate the effects of these structures on the safe surgical trajectory.

2. GENERAL INFORMATION

2.1. Development of Ear

Although the ear has functional integrity, three different parts of the ear that develop from 3 different germ layers. The internal ear develops earlier than the other parts of the ear. It develops from the surface ectoderm opposite both rhombencephalons, the middle ear grows from the 1st pharyngeal pouch endoderm, the external auditory canal origins from the ectoderm of the 1st pharyngeal cleft dorsal, the auricle develops from the mesenchyme behind the 1st and 2nd pharyngeal arches (34, 35). Table 2.1. shows the stages of the development of the 3 parts of the ear.

2.1.1. Internal ear

Embryonic life, around the 22nd day, sees the emergence of the otic placode as the surface ectoderm thickens on both sides of the myelencephalon. Facilitatory signals originating from the paraxial mesoderm and notochord stimulate the surface ectoderm to form placodes. Both otic placodes rapidly penetrate into the mesenchyme located deep within the surface ectoderm. Thus, the otic pit is formed. The primitive form of the membranous labyrinth is the otic vesicle. It is formed by the fusion of the edges of the otic pit. Soon, the contact between the otic vesicle and the surface ectoderm comes to an end. A diverticulum extends from the otic vesicle. This diverticulum eventually forms the endolymphatic sac and duct. Small endolymphatic ducts, utricles and semicircular canals develop from the dorsal utricular part of the otic vesicle, while the cochlear duct and saccule develop from the ventral saccular part. The cochlear duct grows into a tubular diverticula and curves to form the membranous cochlea. The spiral organ, also known as the Corti organ, arises from the specialization of epithelial cells situated along the cochlear duct's wall. The spiral ganglion is formed by the movement of ganglion cells of the eighth cranial nerve (vestibulocochlear nerve) along the folds of the membranous cochlea. With the growth of the membranous labyrinth, the vacuoles are formed in the otic capsule, and with their union, the perilymphatic space is formed. It develops into the perilymphatic space scala tympani, and scala vestibuli associated with the cochlear duct. The otic capsule, which consists of a cartilage structure, ossifies and the bony labyrinth is formed. Thus, the internal ear achieves its adult size and shape by 20-22 weeks of the fetal period (34, 36). Figure 2.1 illustrates the fetal development of the inner ear.

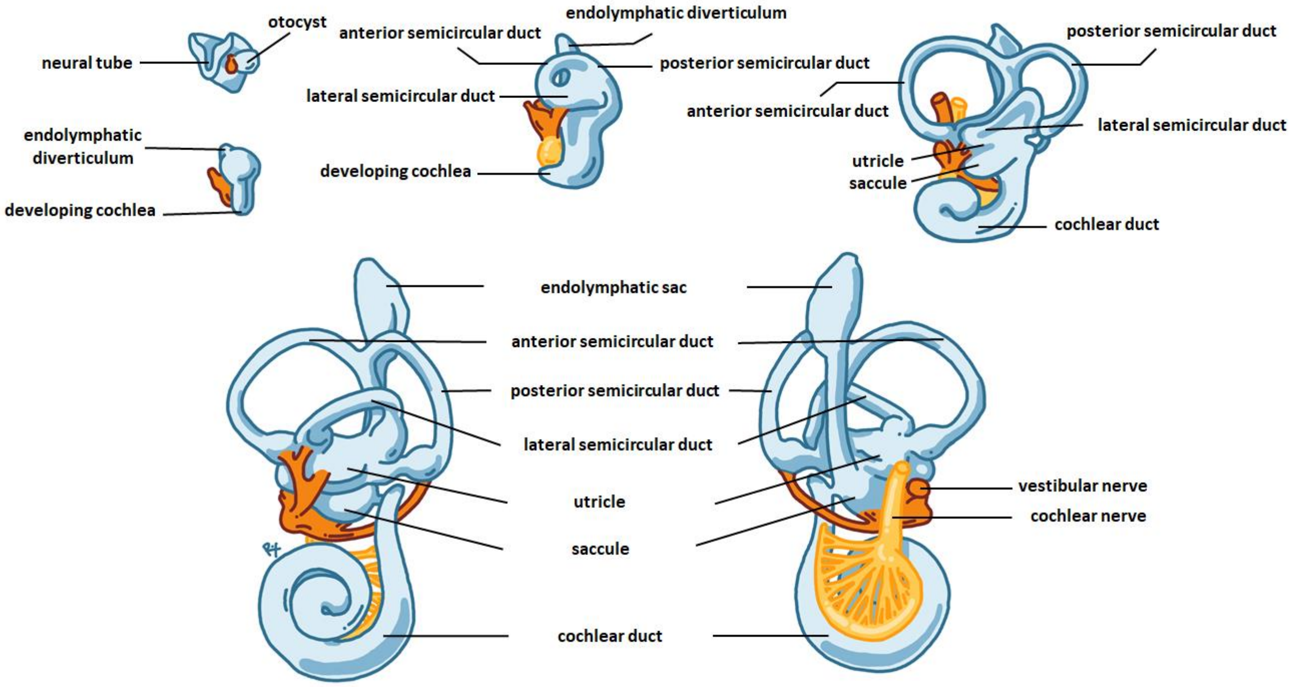

Figure 2.1 Fetal development of the inner ear

2.1.2. Middle ear

The first step in the growth of the middle ear, which begins in the third week, is the lateral developments from the endoderm of the first pharyngeal pouch. Proximal to the tubotympanic recess, its growth from the 1st pharyngeal pouch and forms the pharyngotympanic tube. From the distal section of the tubotympanic recess, a cavity develops that gradually begins to envelop the auditory ossicles, muscle tendons and ligaments, and chorda tympani. The cartilage of the 1st pharyngeal arch is origin for the malleus and incus. Also, stapes arise from mesodermal cells and neural crest. Tensor tympani, one of the two middle ear muscles is originated from mesenchyme in the 1st pharyngeal arch. Besides the stapedius develops from the 2nd pharyngeal arch (34, 36).

Ossicular chain

The initial indications of ossicular chain formation emerge in the human embryo around the fourth week of gestation. From the early stages of embryonic development, stapes undergoes a separation from its intimate association with the remnants of facial nerve and stapedial artery. The contours of the malleus and incus become discernible around the fifth week, coinciding with the condensation of mesenchymal cells (35).

Middle ear cavity

The complete formation of the middle ear space originates from the primitive endoblastic pharyngeal diverticulum situated between the otic capsule medially and the external auditory canal laterally. This diverticulum, known as Köllicker tubotympanic canal, initiates its development during the third week of embryonic life. The progression of the middle ear cavity encompasses three successive stages: the establishment of the primary tympanic cavity, the formation of the tympanic atrium, and the development of the epitympanic recess, antrum, and mastoid cavity (35).

Primary tympanic cavity

The tubotympanic canal takes shape through the evagination of the pharyngeal pocket. The tubotympanic canal's dorsal end concludes beneath the handle of the malleus, below the mesodermal thickening of the ossicular chain. At this point, the tympanic cavity is confined to the lower quadrants exclusively, and this configuration persists until the onset of the second stage around the 20th week (35).

Tympanic atrium

As the tubotympanic canal ascends, it encounters the ossicular chain. The construction of labyrinthine wall of tympanic cavity initiates during this phase of development (34, 35).

Middle ear spaces

Between the third and seventh months, the gelatinous tissue within the middle ear undergoes absorption. Upon completion of this process, middle ear is characterized by the expansion of fluid sacs lined with endothelium, originating from the Eustachian tube opening and extending into the middle ear cleft (35, 36).

2.1.3. External ear

The commencement of auricle development takes place in the fourth week of the embryonic period. The initial configuration of the auricle manifests as thickened tissue extending upward (mandibular arch) and downward (hyoid arch) relative to the first pharyngeal groove (35). It originates from mesenchymal proliferations in the first and second pharyngeal arches surrounding the first pharyngeal groove (34, 36). Although the auricle attains its mature shape by the fifth month, proportional growth continues until the ninth year. Starting from the 4th week of embryonic life, an ectodermal depression occurs dorsal to the first pharyngeal groove. This depression is the first outline of the external acoustic canal. The part of the external acoustic canal surrounding the meatal plate will form the bony part of the external acoustic canal. (35). It is relatively shorter at birth, reaching adult size by the 9th year (36). The external surface of the eardrum is derived from the first pharyngeal membrane. The eardrum originates from 3 different structures; the 1st pharyngeal groove ectoderm, the tubotympanic recess endoderm, a derivative of the 1st pharyngeal pouch, the 1st and 2nd pharyngeal arches mesenchyme (34).

Table 2.1 Fetal development of ear according to weeks

Weeks	Internal	Middle	External
3	Otic placode formation	Tubotympanic recess outline	
4	Otocyst, vestibulocochlear subsection		Thickness of ectoderm
5			External acoustic canal outline
6	Utriculo-saccular subsection		
7	Formation of cochlear basal turn		
8		Cartilaginous incudo-mallear outline	Cartilaginous part of the external acoustic canal
9		Eardrum	
11	Formation of 2.5 cochlear spirals		
12	Cochlear sensorial cells, membranous labyrinth, ossification of otic capsule		
15		Cartilaginous stapes outline	
16		Incudo-mallear ossification	
18		Ossification of stapes	
20	Maturation of internal ear		
30		Tympanic cavity	
34		Mastoid system	
35		Antral cavitation	
37		Epitympanic cavitation	

2.2. Anatomy of the Ear

The ear is an organ of balance as well as a hearing function. It, which is mostly located in the temporal bone and it is generally divided into 3 parts as the external, middle and inner ear. The external ear consists of the auricle and the external acoustic canal. The middle ear is divided into 2 parts as tympanic cavity proper and epitympanic recess. The internal ear is including the bony and membranous labyrinths (36).

2.2.1. Temporal bone

The temporal bone, which is one of the skull bones, contains 3 main parts (*petrous part, squamous part and tympanic part*) anatomically (36). The internal ear is located in the petrous part. The tympanic part encircles the eardrum and forms the antero-inferior wall of the external auditory canal. The squamous part joins the he lateral part of the skull (7).

2.2.2. The facial canal and facial nerve

The facial nerve is divided into 3 parts as intracranial, intratemporal, and extracranial parts. The intratemporal part of the facial nerve is related closely to the tympanic cavity and it leaves the skull by passing via its canal in the temporal bone. It commences with the entry of the facial nerve, along with the intermediate nerve, through the internal acoustic meatus of the temporal bone, into the facial canal situated within the petrous part of the temporal bone. It is divided into four segments and examined as meatal, labyrinthine, tympanic and mastoid segments (Figure 2.2). The facial canal begins as it goes the antero-superior part of the internal auditory canal fundus of the facial nerve. The facial nerve labyrinthine segment continues into the geniculate fossa, where the geniculate ganglion is located. Following the pass to the first genu, the facial nerve gives rise to its first branch, the greater petrosal nerve. In the geniculate fossa, it tends posterolaterally and becomes the tympanic segment. In this segment, the facial nerve is usually straight. The second branch running within the facial canal by the facial nerve is the nerve to the stapedius muscle, providing motor innervation to the stapedius muscle. It is emerging from the mastoid segment of the facial nerve. Another branch originating from the mastoid segment and the final branch of the facial nerve in the canal is chorda tympani. It simultaneously serves as the terminal extension of the intermediate nerve. It traverses through the ossicles in the middle ear and exits the tympanic cavity at the petrotympanic fissure, where it merges with the lingual nerve, a branch of the trigeminal nerve. The mastoid segment of the facial nerve continues from the second genu to the stylomastoid foramen. The facial canal mastoid segment can be easily detected in axial CT and MR sections due to mastoid pneumatization. Excessive pneumatization may complicate CT evaluation (36-41).

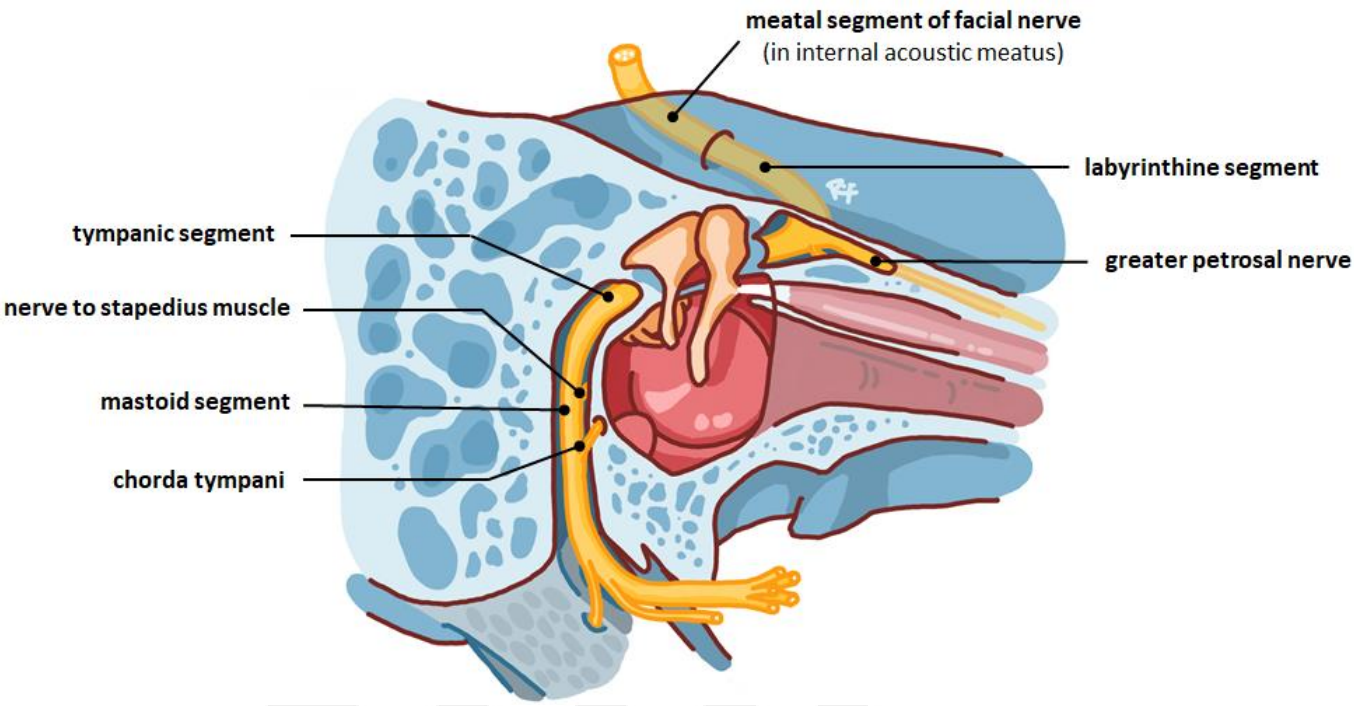

Figure 2.2 Facial canal and intratemporal segment of the facial nerve

2.2.3. External ear

External ear contains the external acoustic canal and auricle. The auricle collects sound waves and conduct to the tympanic membrane through the external acoustic canal. Resembling a large ellipse at the top, the auricula shows many indentations and protrusions, but is concave as a whole. The skeleton of the auricle consists of a fibroelastic cartilage covered with skin. The cartilage is attached to the surrounding structures by means of ligaments and muscles. It is connected to the external acoustic canal by a fibrous tissue. The external acoustic canal continues from the concha of auricle to the tympanic membrane. The external acoustic canal, with an average length of 2.5-3 cm, is not a straight tube, but curved in the shape of an 'S' letter. The outer 1/3 is made up of cartilage (about 8 mm), and the inner 2/3 is made up of bone (about 16 mm) (36, 38).

2.2.4. Middle ear

It is an irregular space located in the temporal bone with a volume of approximately 0.5 cm^3 (Figure 2.3). The tympanic cavity is filled with air as it is connected to the pharynx through the auditory tube. In addition, it contains the ear ossicles and small muscles. It is subdivided into two parts anatomically, the tympanic recess (attic) and the tympanic cavity proper, with an imaginary line passing via the upper boundary of the tympanic membrane (36, 42). In addition, it can be also divided into subcavities based on their relationship to the mesotympanum. Mesotympanum is the part that an observer can visualize through the external acoustic canal using an otoscope. There is the retrotympanum behind, the epitympanum above, the protympanum in front, and the hypotympanum below (35). The middle ear has six walls as roof (*tegmental wall*), a floor (*jugular wall*), an anterior (*carotid*) wall, a posterior (*mastoid*) wall, a lateral (*membranous*) wall, and a medial (*labyrinthic*) wall (36, 38, 42).

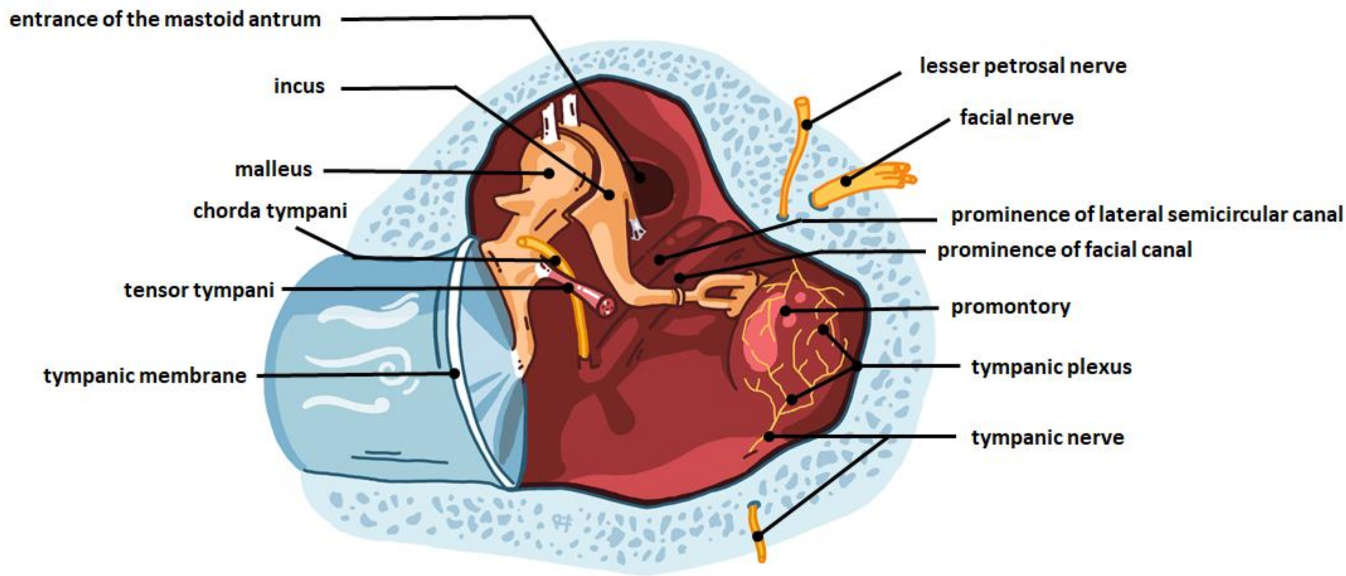

Figure 2.3 Anterior view of the middle ear

Roof

The roof or tegmental wall formed by a thin plate of bone called the tegmen tympani. Tegmen tympani separates the tympanic cavity and the cranial cavity. This wall continues as the ceiling of the canal in which the mastoid antrum is located posteriorly and the tensor tympani anteriorly (36).

Floor

The floor is in the form of a thin and narrow bony partition. The part separates the tympanic cavity and the jugular fossa. The tympanic nerve passes through the opening at the junction with the inner wall (36).

Lateral wall

Tympanic membrane forms most of this wall. A small upper part is formed by the epitympanic recess lateral wall. Tympanic aperture of canaliculus of chorda tympani is located in the corner formed by the outer and posterior walls and just behind the tympanic membrane. This opening is connected to the facial canal via a thin channel, approximately 6 mm above the stylomastoid foramen. A branch of the chorda tympani and stylomastoid artery passes through it and enters the tympanic cavity (36) (Figure 2.4).

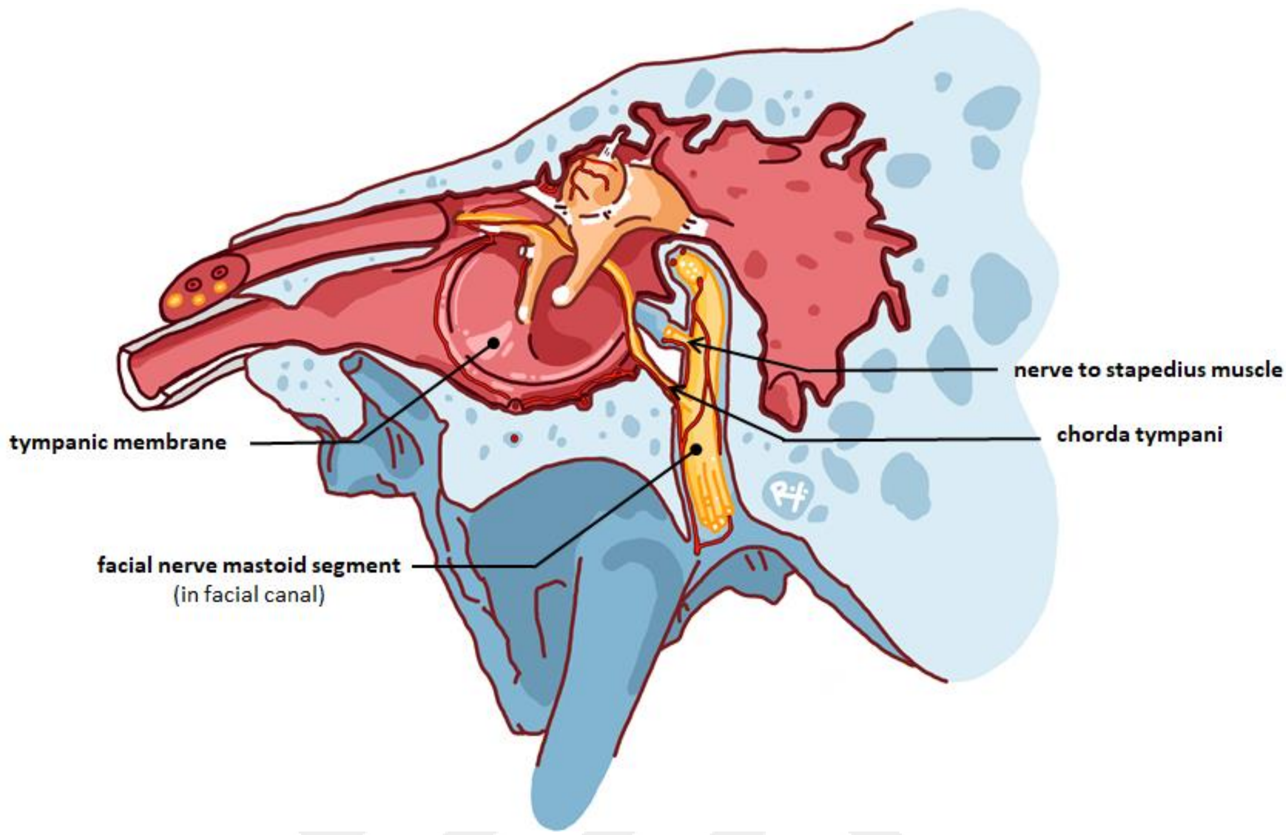

Figure 2.4 The lateral wall of the tympanic cavity

Medial wall

The medial (labyrinthic) wall is also the lateral wall of the vestibulum of the internal ear. There are very important structures such as prominence of facial canal, promontory oval window, and round window on the inner wall (36) (Figure 2.5).

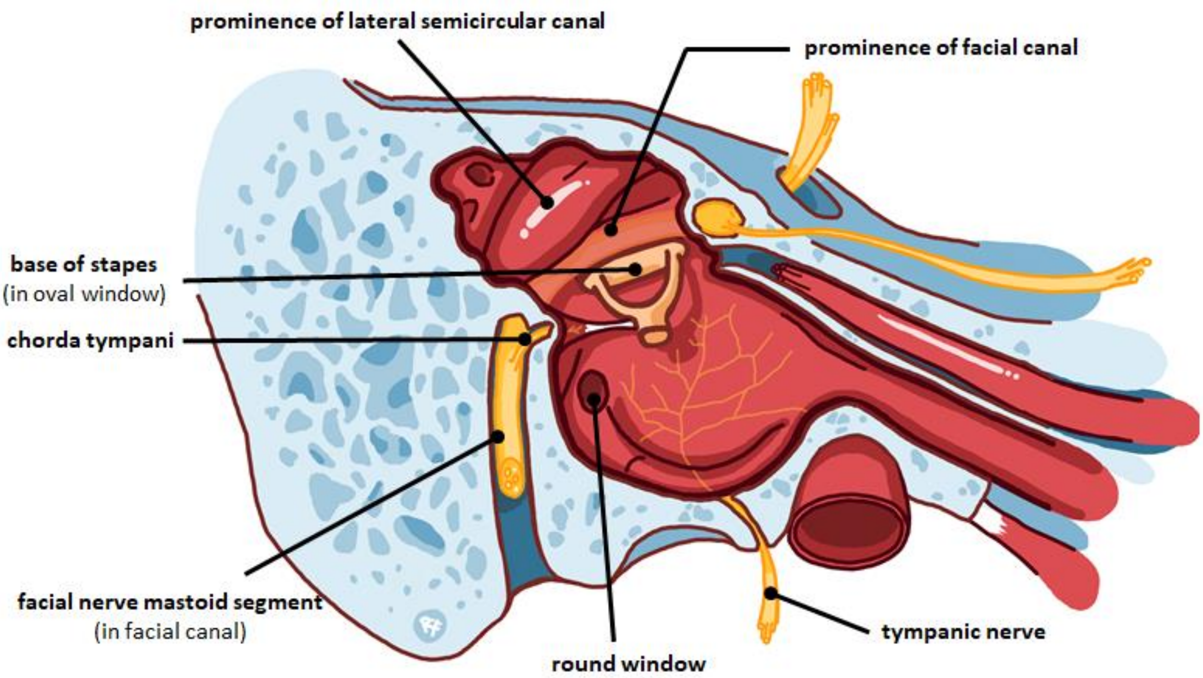

Figure 2.5 The medial (labyrinthine) wall of the tympanic cavity

Oval window: It is shaped like a kidney with its long axis sagittal and its convex edge up, and it connects the tympanic cavity to the vestibulum. The shallow depression in which it is located is called the fossa of vestibular window. The base of stapes sits in this passage located at the back and upper part of the promontory, and these two structures are connected to each other by the annular ligament (36).

Round window: It is located slightly below and slightly behind the oval window. Posterior part of the promontory enters between the round and oval window. The round window is located at the bottom of a funnel-shaped depression, so it is not clearly visible like an oval window. It is closed in vivo by the secondary tympanic membrane. Canonus is defined as a bony eminence that partially envelops and protects the round window (36).

Promontory: It is a protrusion of the cochlear base towards the tympanic cavity. It has groove of promontory on it. In these grooves the fibers of the tympanic plexus sit (36).

Prominence of facial canal: It is a protrusion of the facial canal through to the tympanic cavity. This protrusion extends posteriorly above the oval window on the inner wall, then turns downward and descends on the anterior wall of the mastoid process (36).

Posterior wall

The posterior or mastoid wall contains the aditus to mastoid antrum, pyramidal eminence, and fossa of incus. Aditus to mastoid antrum is a great opening located in the posterior upper part of the tympanic cavity. The opening connects the epitympanic recess to the mastoid cells and antrum. A projection is placed on the medial wall of the aditus to the mastoid antrum. It made by the lateral semicircular canal and the projection is called as prominence of lateral semicircular canal. In front of and below this, prominence of facial canal is located. Facial recess (FR) is defined as the recess between the facial nerve and chorda tympani located on the posterior wall. Pyramidal eminence is a pyramidal projection located in front of the last vertical portion of the facial canal and just behind the sinus tympani and oval window. The stapedius muscle is situated in this prominence. Pyramidal eminence is connected to facial canal by a thin canal. A thin branch of the facial nerve passes through this canal, which innervates the stapedius muscle (36).

Anterior wall

The carotid canal is situated anterior to tympanic cavity. Consequently, the wall is also called the carotid wall. A delicate bony partition exists between the tympanic cavity and carotid canal. The internal openings of the two channels are opened on the upper section of anterior wall. And there is a thin bony plate between two canals. The superior canal is semicanal for tensor tympani, and the bottom one is semicanal for auditory tube (36).

Auditory ossicles

In the middle ear, there are 3 moving ossicles: malleus, incus and stapes, which transfer general vibrations to the eardrum and to the inner ear. The malleus sits on the eardrum and stapes sits on the oval window. Incus articulates with the other two ear ossicles. Ear ossicles reduce the movement of the eardrum 15-20 times, but increase the power at the same rate. Frequency does not change. The malleus is the largest ear ossicle. It has two parts, head and neck, and 3 projections, lateral and anterior process and handle. Incus has a body (body of incus) and two projections (long and short limbs of incus). Stapes has a head (head of stapes), two arms (anterior and posterior limbs of stapes) and a base (base of stapes) (36, 38).

There is a saddle joint between the malleus and incus, and a spheroid joint between incus and stapes. In addition, base of stapes is seated on oval window in such a way that it can move with the annular ligament. This movement is controlled by the stapedius muscle (36).

Auditory muscles

Two muscles control the movement of the auditory ossicles. Tensor tympani locates the canal above the pharyngotympanic tube. The mandibular nerve's medial pterygoid branch provides innervation to this muscle. The stapedius muscle is situated within the pyramidal eminence. Innervation of the stapedius muscle is carried out by a facial nerve branch (36, 38).

2.2.5. Internal ear

The internal ear locates within the petrous portion of temporal bone, contains specific cells responsible for both hearing and balance. It comprises two interconnected components, the osseous and membranous labyrinth (36, 38).

Bony labyrinth

Bony labyrinth is larger than the membranous labyrinth therefore there is a cavity between them (Figure 2.6). This cavity contains the perilymph. In children, this fluid is associated with cerebrospinal fluid. Bony labyrinth has 3 parts: vestibule, semicircular canals and cochlea. Middle part of the bony labyrinth is formed by vestibule. There are three semicircular canals as anterior, posterior and lateral. These canals are situated in the posterior upper part of the vestibule. The semicircular canals and vestibule contain specific cells involved in balance (38).

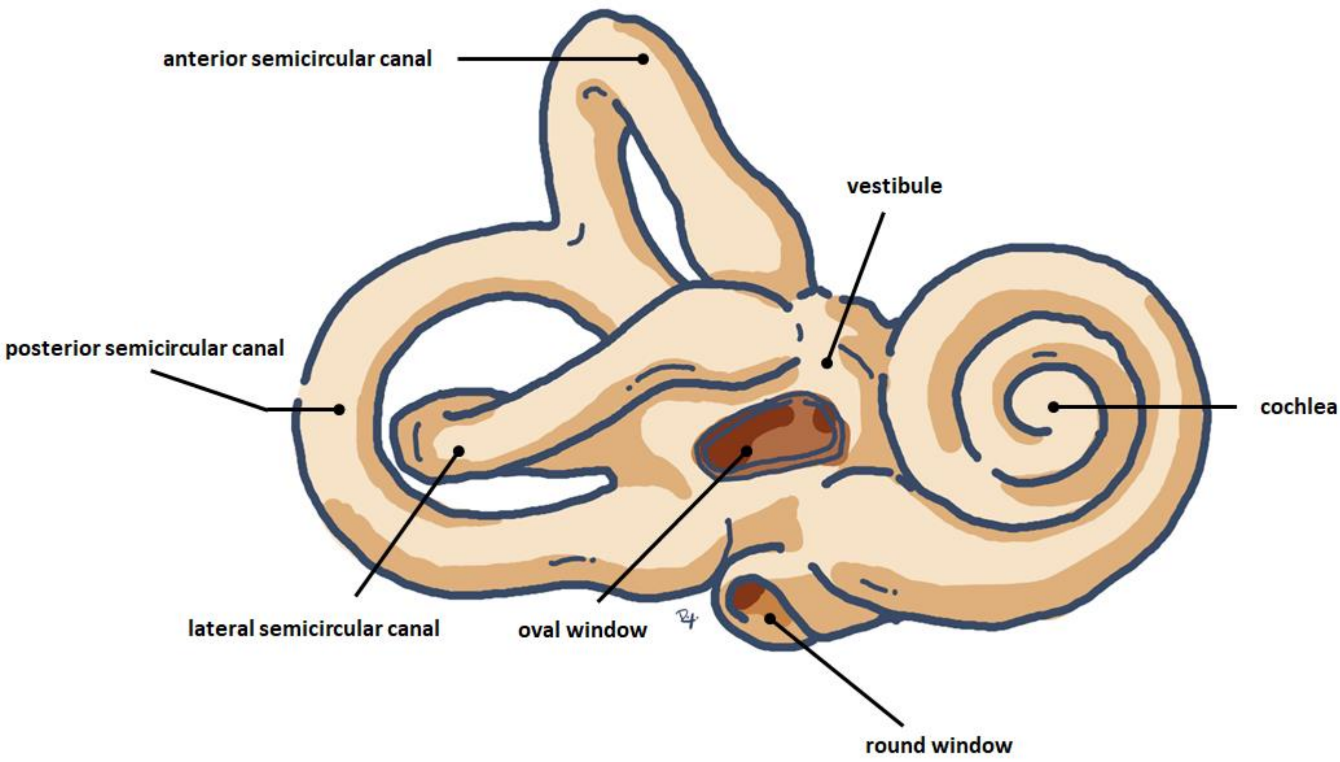

Figure 2.6 Bony labyrinth

Cochlea

It is located in the anterior inner part of the cochlea vestibule, which is shaped like a snail (Figure 2.6). The cone-like cochlea is about 9 mm in diameter and 5 mm in height. Its apex (cochlear cupula) faces anteriorly and outwardly and projects anteriorly to the superior part of the tympanic cavity's medial wall. Its base (base of cochlea) coincides with the tractus spiralis foraminosus at the bottom of the internal acoustic canal. The perforated cone-shaped structure seen in the middle in a cross-section made from the apex to the base is called the modiolus (Figure 2.7). Spiral canal of cochlea goes around the modiolus 2.75 times. Cochlear duct is located within the bony spiral lamina. It connects to the modiolus at one end and the outer cochlear wall at the other. As a result, three longitudinal canals occupy the cochlea. The cochlear duct, also known as the scala media, terminates blindly at the apex of the cochlea. Two flexible membranes delineate the upper and lower boundaries of the cochlear duct. These are vestibular and basilar membranes. The vestibular membrane acts as the barrier between the scala media and scala vestibuli, while the basilar membrane serves as the divider between the scala media and scala tympani. The organ of Corti is situated on the inner surface of the basilar membrane. Positioned at the base of the scala vestibuli, the oval window serves as an entrance to the vestibular cavity. It is sealed by the base of the stapes. Separating the scala tympani and the tympanic cavity is the secondary tympanic membrane at the round window (36, 42).

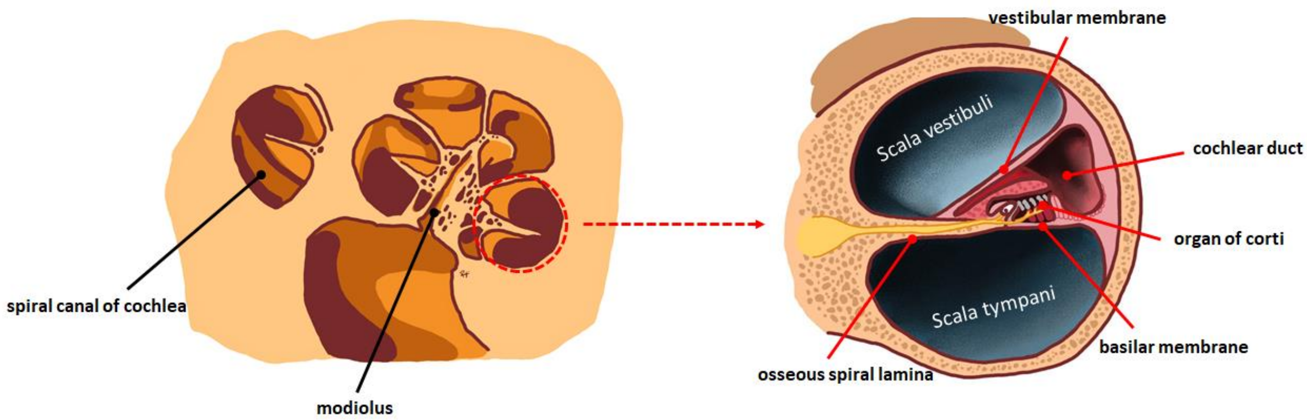

Figure 2.7 Modiolus and organ of corti

Organ of Corti

The discovery of the organ of Corti dates back to the work of Italian physician Domenico Cotugno 100 years ago. (43). The organ of Corti is positioned within the scala media (cochlear duct) and on basilar membrane medial part. This membrane constitutes the lower boundary of the scala media and manifests as a protrusion in histological transverse sections. Cells within the organ of Corti are categorized into support and sensory cells, arranged in two rows: internal and external. Sensory cells are made up of a series of electromagnetic sensitive cells called hair cells. Hair cells are of two types, internal and external hair cells. The base and margins of the hair cells synapse with the ganglion cells of the cochlear nerve. In the cochlea, there are approximately 3500 inner hair cells and around 12000 outer hair cells (36, 44).

2.3. Sensorineural Hearing Loss

Worldwide, approximately 50 million adults have severe or profound hearing loss. Hearing loss is of two types: sensorineural hearing loss (SNHL), which is the type due to damage to the cochlea and cochlear nerve, and conductive hearing loss, which is the type due to damage to the structures that transmit sound to the cochlea. There are many causes that can cause sensorineural hearing loss (SNHL). For most of these reasons, damaged hair cells in the cochlea cannot convert acoustic energy into neural potentials to be sensed by the central nervous system (9). SNHL is the most common sensory defect in more developed societies. At least one in every 1000 children is born with bilateral SNHL (1).

According to etiology more than half of the children born with SNHL have the inherited disorder. In many cases, both parents do not have hearing loss, but the child has non-syndromic SNHL because of Mendelian recessive inheritance. In addition, autosomal dominant, X-linked, and mitochondrial contributions to the load of inherited congenital SNHL may occur. It has been reported that mutations in the GJB2 gene are accountable for almost half of the hereditary SNHL cases in the most of European countries and USA (45-48). Allele variants of GJB2 that cause hearing loss alter the function of the Connexin 26 (an encoded protein in the internal ear) (49, 50). Bacterial meningitis is most commonly caused by acquired SNHL in infants and children. Post-meningitis SNHL may be bilateral or unilateral, however bilateral loss is little more widespread (51). In adults, SNHL can occur due to autoimmune diseases, cerebello-pontine angle tumors, infections such as meningitis and labyrinthitis, Meniere's disease, noise exposure, ototoxic exposure, and trauma (52).

Diagnosis of SNHL contains evidence of decreased hearing acuity by physical examination as well as auditory tests (1, 52). In the treatment of SNHL, hearing aids and cochlear implants are preferred according to the patient's condition and etiology. Hearing aids transmit the sound they receive from the environment to the hearing aid's telecoil or special headphones using different systems. Cochlear implants are recommended for treating hearing loss when patients meet specific criteria, have limited success with hearing aids, exhibit no middle ear ailments, and possess the cognitive capacity to utilize them (52).

2.4. Cochlear Implant

Globally recognized as a cutting-edge treatment, cochlear implants are deemed highly effective for individuals experiencing severe hearing loss (7). It is an undersized and complicated electronic device that restores hearing to people with hearing loss (6).

2.4.1. History of the cochlear implant technology

The idea of acquiring hearing with electrical stimulation was first proposed by Benjamin Franklin in 1751 (7). Later, in 1800, Count Alessandro Volta inserted metal rods into the ear and attached them to a circuit where he developed electrolytic cells (53). Volta created a sound sensation, depicted as the sticky liquid boiling (54). Later, interest in the subject resumed in the second half of the 19th century. A number of cases of tinnitus have been treated by Politzer with electrical stimulation. Wever and Bray found that electrical potential is generated in the cochlea by acoustic stimulation in 1930. Stevens produced tones, which he called the electrophonic effect, with his experiments in 1937, and produced audible frequencies with an electrode using alternating current. The electrode and skin surface functioned as the two plates of a capacitor microphone, transmitting the generated vibrations to the cochlea through a combination of air and bone conduction, resulting in auditory perception (7). Gersuni and Volokhov (55) defined hearing sensations by providing stimulation from the round window of the patient with an electrode. Cochlear implant came into clinical use in the early 1990s. It was initially used as a treatment in patients with severe bilateral hearing loss. However, developments in cochlear implantation surgery in the last 35 years have significantly expanded the indications and age limits of cochlear implants (56).

2.4.2. Cochlear implants: components and working principles

Cochlear implant contains an external portion attached speech processor and second portion placed subcutaneously on the surface of mastoid process (6, 9, 52). A cochlear implant has the following parts (Figure 2.8):

- The microphone collects voice from the environment
- The speech processor specifies and sets voices collected by the microphone
- The transmitter and receiver/stimulator acquire signals from the speech processor and convert the signals into electrical impulses
- The electrode array is an electrode groups that collects the impulses from the stimulator and sends the impulses to the auditory nerve

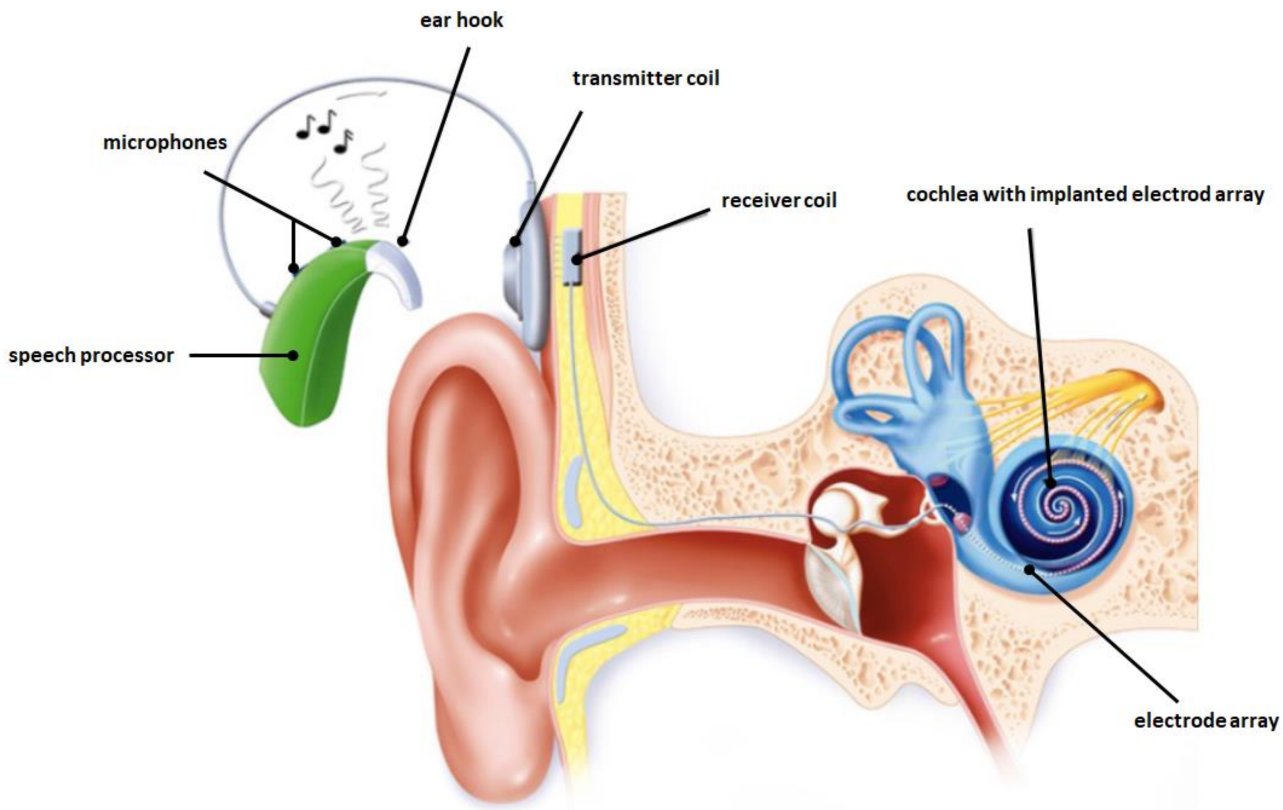

Figure 2.8 Components of the cochlear implants

The sound processor is positioned at the rear of the ear, while the pliable electrode array is inserted into the cochlea (Figure 2.8). A cochlear implant system circumvents the impaired hair cells through the utilization of electrical pulses that convey sound signals initially to the spiral ganglion and subsequently to the cochlear nerve, also referred to as the auditory nerve (6, 7, 54). In order to achieve this, the sound processor identifies ambient sounds and converts them into coded electrical signals through digital means. Subsequently, these signals are transmitted through the skin to the implant via a communication coil. The implant decodes the coded signals into electrical pulses, which are then conveyed along the electrode array to stimulate specific regions of the cochlea responsible for distinct pitches. This targeted stimulation encompasses the entirety of the cochlea, resulting in improved sound quality and a more natural hearing experience. These impulses mimic the actual function of hair cells and can transmit the impulse to the spiral ganglion or auditory nerve. The auditory nerve then transmits these signals to the brain (7).

Possibly the crucial element in cochlear implant surgery involves the insertion of the electrode array into the cochlea. The type of electrode is important in terms of adapting to the patient's condition and the variable anatomy of the cochlea. The amount of angular placement and the cochlear frequency field they cover in the cochlea are the two main reasons why the electrode arrays differ from each other. In addition, special electrodes are preferred for the risk of cerebrospinal fluid leakage in cases with cochlear anomalies. Accordingly, the electrode arrays have different designs according to the contact types (7).

2.5. Cochlear Implantation Surgery

It is thought that the large cortical mastoidectomy and a wide posterior tympanotomy are the golden standard for cochlear implantation surgery (10). Cochlear implantation surgery involves the mastoidectomy and posterior tympanotomy approach (MPTA), followed by placement of the electrode array into the cochlea through either the round window approach or the cochleostomy (11). During this procedure, a recommended technique is the utilization of a limited access keyhole for the cochlear implant, involving a progressively smaller incision for a 2 cm retro-auricular flap. The mastoid process cortical part behind the external acoustic canal remains exposed and untouched. The initial drilling towards the mastoid antrum is guided by landmarks such as Henlé's spine and Mac Ewen's triangle. The temporal line, positioned at the superior boundary of the mastoid process, serves as a landmark for the level of the middle fossa dura. A platform for the placement of the cochlear implant's electronics package is created in the superior-posterior direction using a periosteal elevator (11, 57).

Cortical mastoidectomy, which is the basic operation in temporal bone surgery, is defined as the exenteration of the mastoid process without compromising an anatomical integrity of external and middle ear (11). A faster drill provides a more secure mastoidectomy compared to the previously employed chisel (10). facia electrode array to the cochlea is started through a cochleostomy or round window. If the cochleostomy technique is to be used to access the cochlea, the cochleostomy is performed around 1-2 mm from the round window anterior-inferior part. To access the cochlea from the round window, the secondary tympanic membrane must be pierced. The receiver-stimulator package must be fixed in the drilled well before electrode array is inserted. Finally, the most sensitive part of the surgical procedure is completed by placing electrode array via mastoid space, posterior tympanotomy and via round window or cochleostomy into the cochlear basal turn (7, 10, 11).

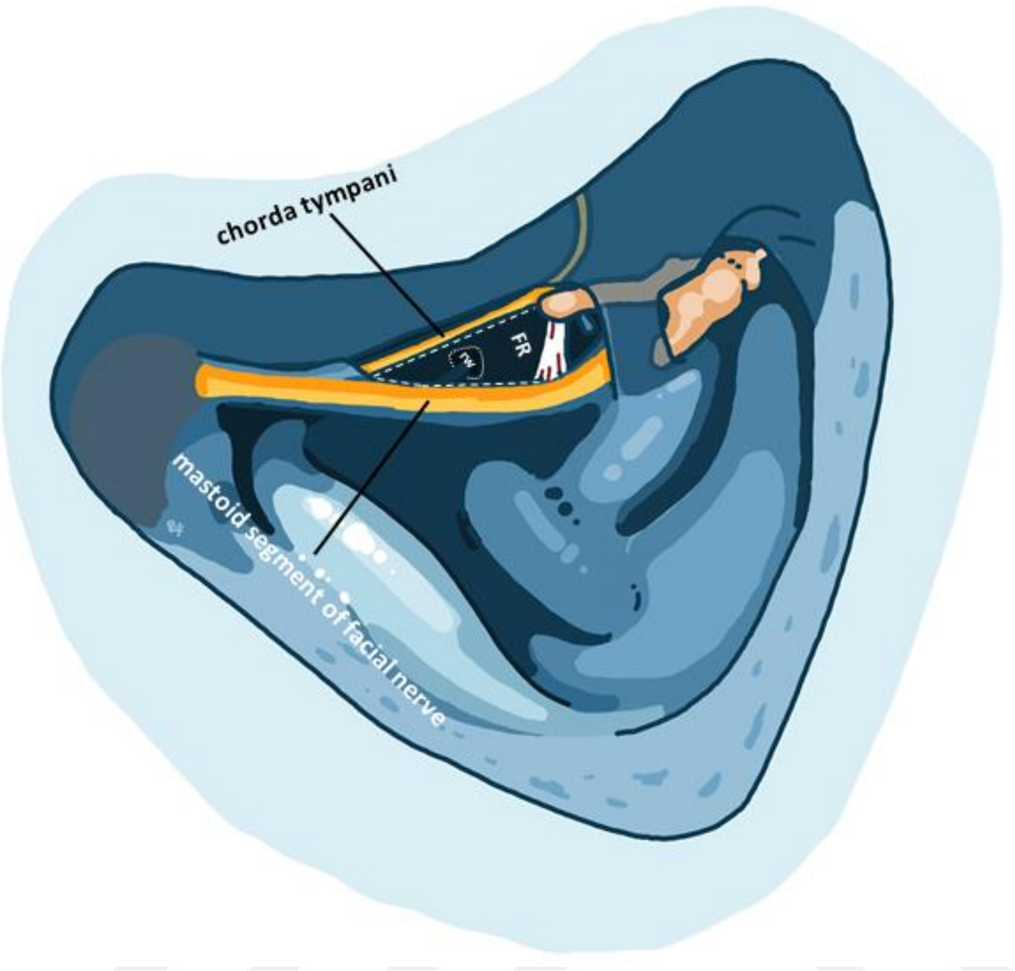

Figure 2.9 Exposure of the FR after the cortical mastoidectomy

FR: Facial recess, rw: Round window

2.5.1. Robot – assisted cochlear implantation surgery (RACIS)

Robot-assisted cochlear implantation surgery (RACIS) contains 3 main stages: middle ear entrance, internal ear entrance, and electrode array placement. The ultimate purpose of robot use in this surgery is the fully robotic automation of all stages (58). In the last 15 years, different studies have been conducted on the various components of robot use in cochlear implant surgery (3, 5, 19, 58-65). Different components were studied, such as the design of the robot and the development of safety mechanisms, and finally the first study combining all these components into a single robot was published by Weber et al. (5) in 2017. The development of the RACIS was of course dependent on advances in imaging technologies (Figure 2.10). Preoperative imaging and 3D reconstruction of the middle and internal ear structures help determine whether safe access to the patient's round window can be achieved (58). For preoperative evaluation, the middle and internal ear structures of the patient are reconstructed via computerized tomography images through the OTOPLAN, (CASCINATION AG, Bern, Switzerland) program. All anatomical factors, including facial recess dimensions, cochlear sizes, and cochlear approach angles, are segmented. A simulation of the trajectory is conducted using the OTOPLAN®. Facial recess' mean dimensions are 2.54 ± 0.5 mm. To securely reach the round window, the 1.8 mm diameter bur should pass the safe distance from both chordae tympani and facial nerve (58, 66). Today, the safe distance to avoid facial nerve palsy is considered to be 0.4 mm (3, 58). The first step of surgery with RACIS is to place the patient's head on an atraumatic headrest. After a retro-auricular incision, approximately 4 reliable screws are placed on the mastoid surface. These screws are important for providing reference points during intraoperative imaging. After the previously planned safe trajectory is reaffirmed via OTOPLAN®, the surgery continues. During the initial phase of autonomous access to the middle ear, robotic drilling occurs from mastoid surface to around 3 mm in front of the anticipated depth of facial nerve. Drilling halts about 3 mm before reaching the anticipated depth of the facial nerve. Subsequently, an initial intraoperative CT scan is conducted to assess the drilling trajectory and identify any discrepancies. In the imaging process, the titanium rod is placed into the drilled cavity to trace the trajectory within the surrounding anatomy. Intraoperative imaging is conducted using a portable CBCT device. As a result of the imaging, the drilled trajectory and the planned trajectory are compared and it is decided whether to continue drilling or not. The most crucial phase in gaining access to the middle ear is the second stage. During this phase, the facial recess undergoes drilling. It is crucial to maintain a minimum distance of 0.3 mm from chorda tympani and 0.4 mm from facial nerve. The third and fastest step continues until the drilling arrives the middle ear. This stage is the least risky stage (58). The next and second stage is autonomous internal ear access. At this stage, a 1 mm drill burr is used instead of a 1.8 mm burr. The internal ear access process is the milling of the canonus, the bony prominence of the round window (42). Canonus thickness is calculated by preop imaging. In addition, lateral and medial borders were defined by preoperative imaging. As a result of canonostomy, the 0.8 mm diameter electrode array can pass from approximately canonostomy which has a 1 mm diameter. The autonomic inner ear access process takes place in 4 stages. Phase 1, referred to as the touchdown, involves the drill making contact with the canonus' lateral wall. Phase 2, the plateau phase, occurs when the drill burr is fully within the canonus. Phase 3, the breakthrough phase, initiates when the drill burr reaches the canonus' medial wall. In Phase 4, the enlarging phase, the drill is intended to penetrate 0.3 mm beyond the edge of the medial wall. Consequently, a canonostomy with a diameter of 1 mm is performed so that the 0.8 mm electrode can pass smoothly (3, 58). Autonomous electrode placement, which is the final stage of robotic cochlear implantation, has not yet taken place in practice (58). Despite this, the RobOtol® and iotaSOFT® systems can ensure that a equator is placed at a given speed (67, 68). However, none of these yet guarantee a standard insertion into the inner ear with a right angle (58). This stage is still accomplished manually by the surgeon in the HEARO procedure (3, 58).

Figure 2.10 The HEARO® robotic system.

1. Robot mount, 2. Headrest, 3. Patient marker attachment, 4. Patient marker, 5. Drill, and 6. Drill mount with force/torque sensor (3)

2.5.2. Surgery trajectory angles

The ideal insertion trajectory in cochlear implant surgery is defined as a line parallel to the central line of ST at the level of secondary tympanic membrane. The trajectory aims to minimize the risk of causing harm to the basilar membrane, modiolus, or spiral ligament during the insertion process (10). Wimmer et al. (26) described two angles describing deviations from the ideal trajectory in two different planes. The in-plane angle denotes the variance between the planned and ideal trajectories in relation to the basal turn of the cochlea for a specified target. Additionally, this angle can be defined as the angle between the planned trajectory and an axis parallel to the ST in the inferior view. Certainly, the planned trajectory is passing from the facial recess. Consistently, the out-plane angle is a deviation between the planned and calculated ideal trajectory at basal turn in an orthogonal plane. Also the angle can be defined as the angle between the planned trajectory and the axis passing parallel to the ST in the anterior view (21, 26) (Figure 2.11).

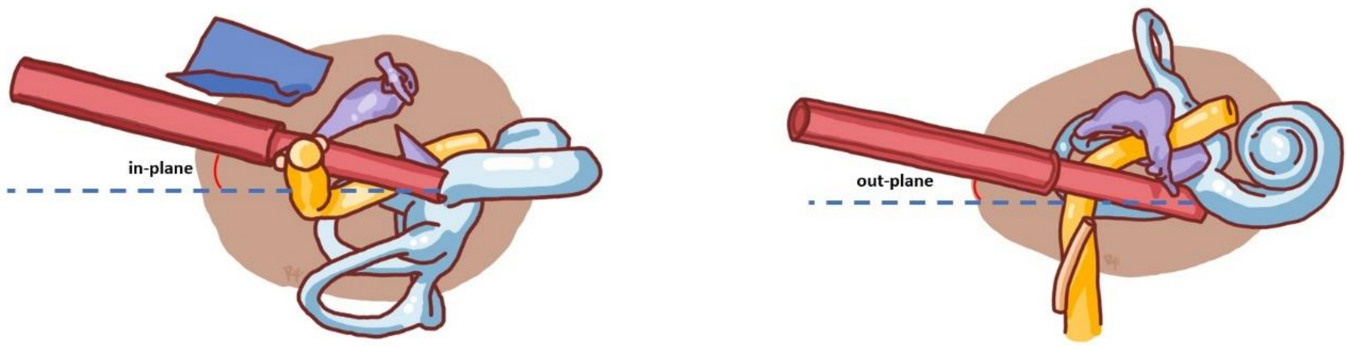

Figure 2.11 Illustration of the surgery trajectory angles

2.5.3. Electrode insertion angles

The precise positioning of an electrode array inside the ST is essential for achieving favorable hearing outcomes (7, 29-32). The optimal placement of the electrode array is considered achieved when the closest active electrode makes full contact within the cochlea, preferably near the round window or cochleostomy. The degree of insertion depth for the electrode array is quantified by the radial position of the end, ranging from 45° to a theoretical maximum of 900° (7). The individual shape and dimensions of the cochlea play a crucial role in determining the position of the cochlear implant electrode array (31, 32). Many studies have reported a significant correlation between insertion depth and cochlear dimensions (69, 70). As a result, preoperative assessment of cochlear dimensions and insertion depth is crucial for selecting the appropriate electrode for each patient (65). Postoperative radiological imaging confirms insertion depth and full insertion (7). The DICOM viewer, which analyzes magnetic resonance imaging and computed tomography images for both preoperative and postoperative evaluation, was used as standard until 2018. CAScination AG, a Swiss company collaborating with MED-EL, introduced OTOPLAN, an otologic software that analyzes preoperative and postoperative radiological images in 2018. OTOPLAN software allows to the examination of the anatomical structures of the middle ear with preoperative 3D reconstruction, as well as to calculate the postoperative electrode insertion depth degree (Figure 2.12) (3, 7).

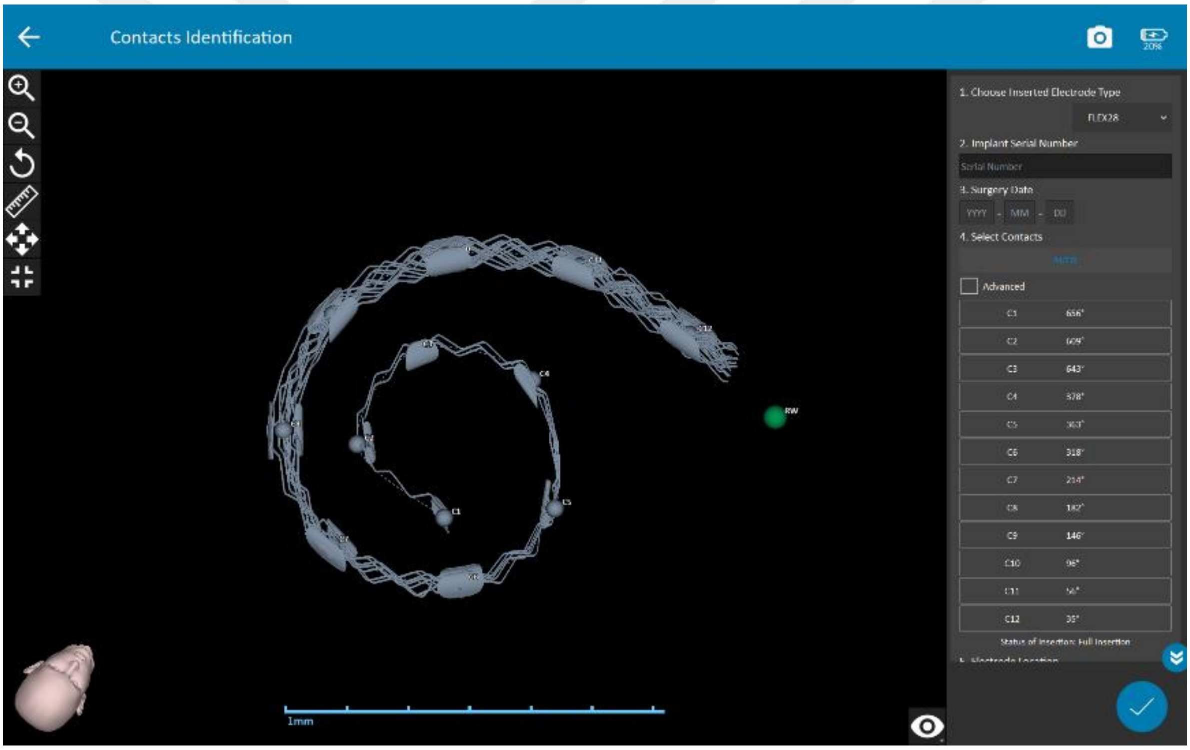

Figure 2.12 Calculation of the postoperative electrode insertion depth degree

3. MATERIAL AND METHOD

Preoperative and postoperative CBCT and HRCT of patients who underwent robotic and conventional cochlear implant surgery at UZ Brussel Hospital were included. The inclusion criteria were patients' images using the MED-EL electrode and who had not undergone prior temporal bone surgery as inclusion criteria were determined. The exclusion criterion was determined as images with low image quality in which anatomical landmarks determined for measurement could not be determined. Ethical approval was obtained from Medical Ethics Committee UZ Brussel Hospital with number 1432022000187.

Robot-Assisted Cochlear Implantation Surgery

Robot assisted cochlear implantation surgery (RACIS) have been performed with the HEARO procedure. Intraoperative imaging could not guarantee a safe distance to the facial nerve in one of the 3 patients, the other 2 patients have been converted to conventional surgery because of software issue, the remaining 22 patients underwent the HEARO procedure successfully (3).

Conventional Cochlear Implantation Surgery

Conventional surgery (CS) has been performed in 33 patients by the same surgeon using MPTA. MED-EL Flex 28 electrodes were used in all patients.

3.1. 3D Reconstruction of the Temporal Bone, Middle Ear and Cochlea

OTOPLAN, (CASCINATION AG, Bern, Switzerland) was used for 3D reconstruction of the temporal bone, auditory ossicles, facial nerve, chordae tympani, cochlea and round window. CBCT and HRCT images in DICOM format were transferred to OTOPLAN.

3.1.1. Measurements of cochlear sizes

Cochlear measurements have been performed in cochlear view. Cochlear view is the view defined as a double-oblique coronal view of the cochlea, in which the RW center is set to 0° with the coordinate system of the cochlea.

- ***Anatomical landmarks for cochlear length (CL):*** Distance between the centre of the round window and the furthest point on the opposite wall of the cochlea on the coronal section of cochlear view (Figure 3.1a-b)
- ***Anatomical landmarks for cochlear width (CW):*** Distance between inferior and superior point of the lateral wall on the coronal section of cochlear view (Figure 3.1a-b)
- ***Anatomical landmarks for cochlear height (CH):*** Distance between the centre of the cochlear base and apex of the cochlea on the axial section of cochlear view (Figure 3.1c-d)
- ***Cochlear duct length (CDL)*** was calculated with OTOPLAN automatically according to cochlear size with the method described by (71).
- ***Basal turn length (BTL)*** was calculated using a method proposed by Escudé et al. (72) $L = 2.62 \times CL \times \log_e (1.0 + \theta/235) = 2.43 \times CL$

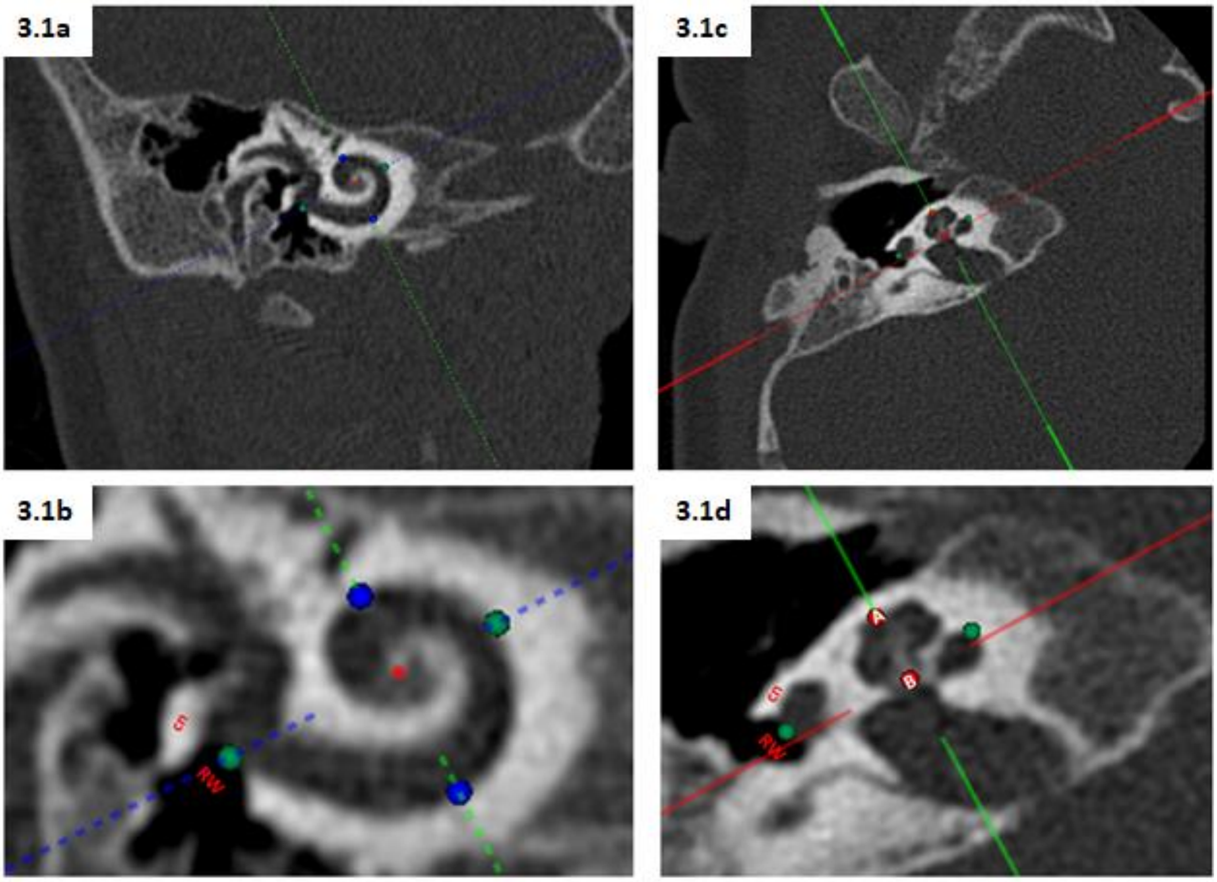

Figure 3.1 Measurement of the cochlear size

RW: Round window, cn: Canonus, A: Apex of the cochlea, B: Base of cochlea

3.1.2. Measurement of round window sizes

Measurements have been performed in the coronal and axial sections of cochlear view.

- ***Anterior-posterior distance of round window (RWAP):*** Distance between two end points (anterior and posterior points) of round window on axial view (Figure 3.2a).
- ***Superior-inferior distance round window (RWSI):*** Distance between two end points (superior and inferior points) of round window on coronal view (Figure 3.2b).

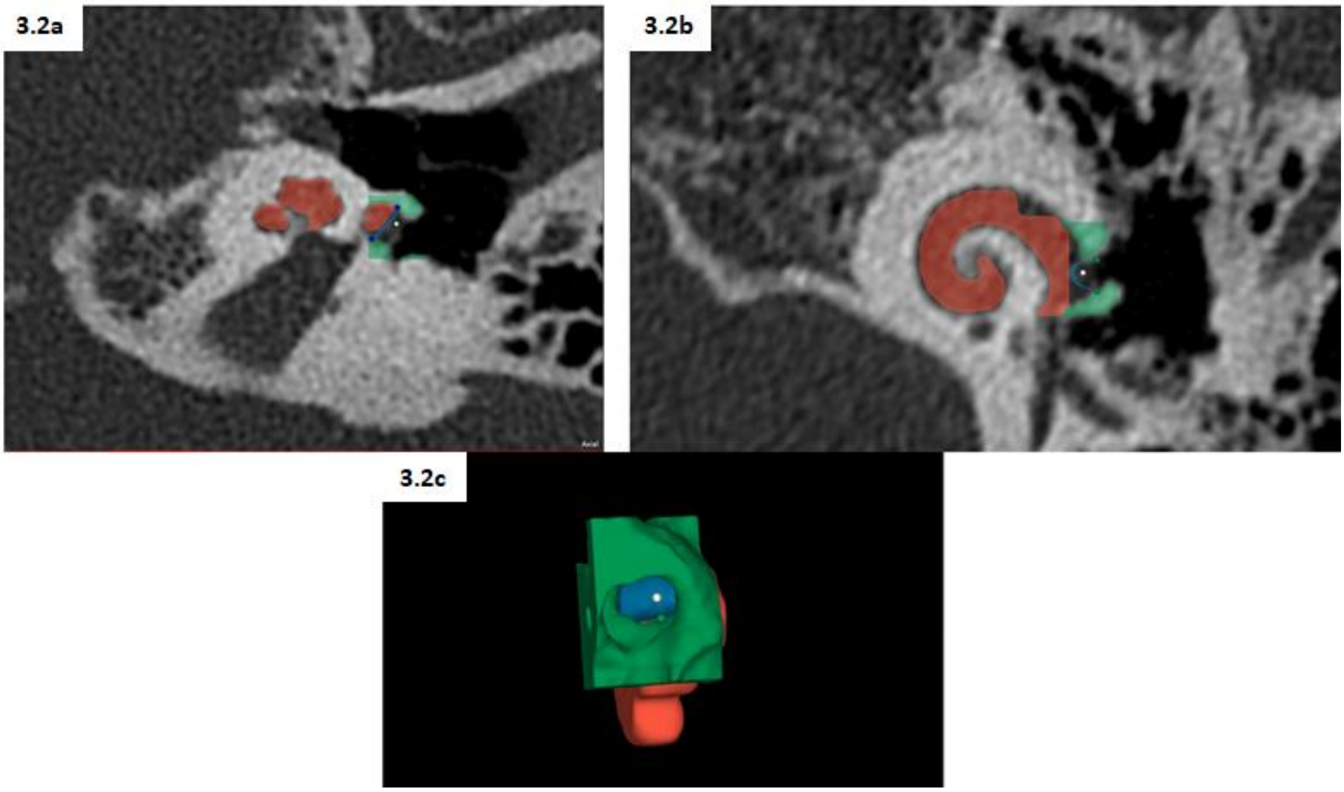

Figure 3.2 Measurement of the round window size

3.1.3. Measurement of canonus sizes

Length of canonus (LC), thickness of canonus (TC) was measured by RadiAnt DICOM Viewer 2023.1. Measurements have been performed in the axial sections of cochlear view. For examiner reliability, measurements were made a second time by the same observer, one month apart.

- ***Length of canonus (LC):*** Distance between start and end point of canonus in axial section (Figure 3.3b)
- ***Thickness of canonus (TC):*** Anteroposterior distance of the thickest part of canonus in axial section (Figure 3.3b)
- ***Canonus type (Ct):*** Canonus was typed as hook (Figure 3.3c) or flat (Figure 3.3d) according to its shape

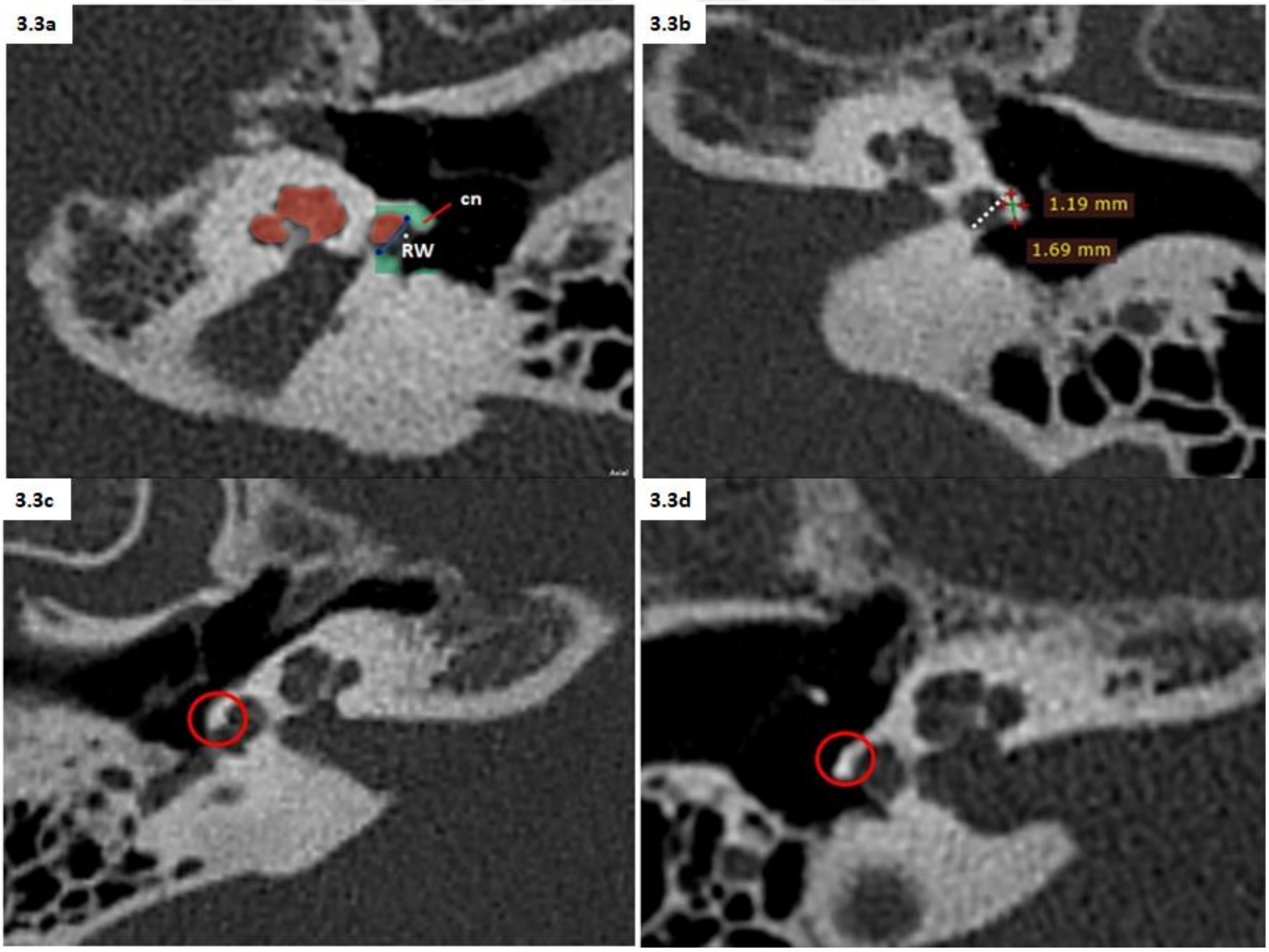

Figure 3.3 Measurement of canonus size

RW: Round window, cn: Canonus, white dashed line: RW membrane

3.1.4. Measurements of angles relations with cochlear orientation

Basal turn angle and cochlea apical angle has been measured by RadiAnt DICOM Viewer 2023.1. For examiner reliability, measurements were made a second time by the same observer, one month apart.

- ***Basal turn angle (BTA):*** The angle between the line passing through the basal turn and the midsagittal plane on the first axial section, where the entrance to the round window and cochlear base was most clearly visible (Figure 3.4a).
- ***Cochlea apical angle (CAA):*** The angle between the line passing through the apex of the cochlea and the midsagittal plane on the first axial section, where the apex of the cochlea and cochlear base was most clearly visible (Figure 3.4b).

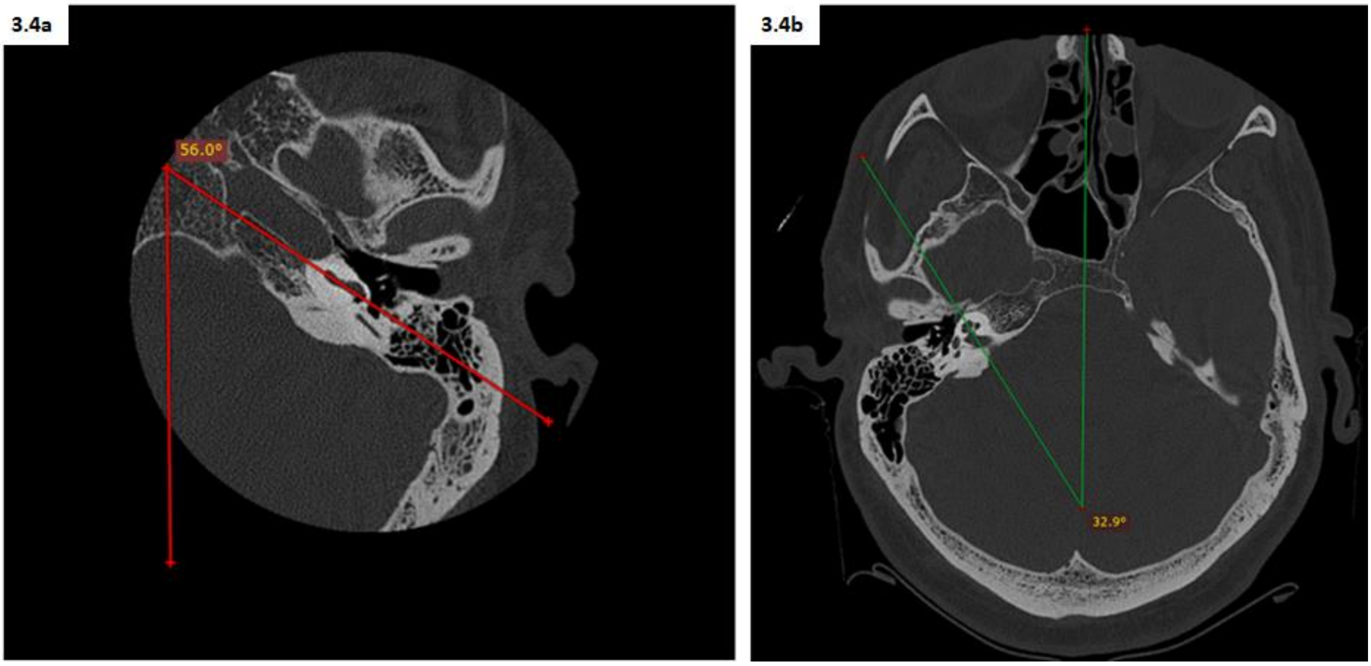

Figure 3.4 Measurements of angles relations with cochlear orientation

3.1.5. Measurements of facial recess width (FRW), facial recess angle (FRA) and depth of the facial nerve mastoid segment (DFNM)

Facial recess width (FRW) was measured automatically with 3D reconstruction made by OTOPLAN. For 3D reconstruction, facial canal was determined in coronal sections and markings were made along the canal. Again, in the coronal section, marking was made along the course of the chordae tympani originating from the facial nerve (Figure 3.5). Facial recess angle (FRA) was measured on the 3D image obtained after the reconstruction of the facial nerve and chordae tympani. Digital image analysis program ImageJ (ImageJ; US National Institutes of Health, Bethesda, MD) was used for angle measurement.

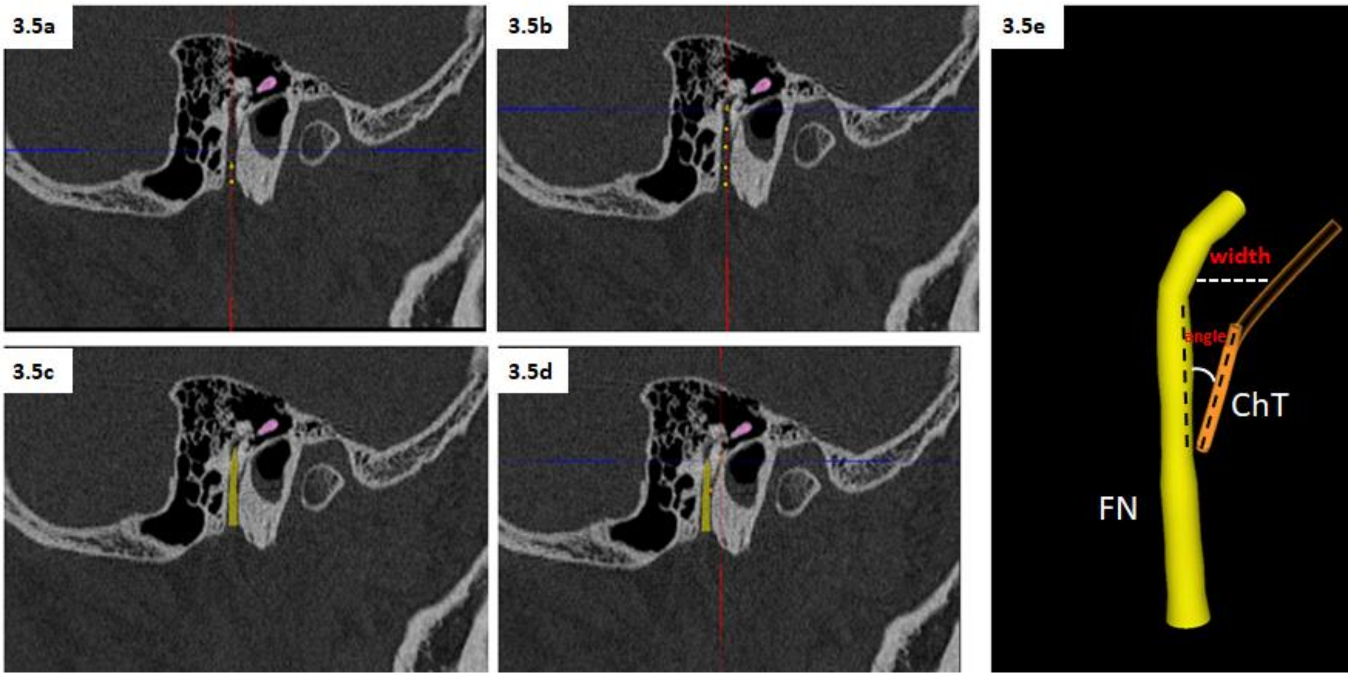

Figure 3.5 Measurements of FRW and FRA

FN: Facial nerve, ChT: Chorda tympani

The depth of the facial nerve mastoid segment (DFNM) has been measured on axial CT slices (Figure 3.6). The coronal section was detected in which the mastoid segment of the facial nerve and the chorda tympani began to appear together for the first time. In the axial section corresponding to this section, the distance between the facial nerve mastoid segment and the lateral surface of the mastoid process has been measured. The measurement was made via RadiAnt DICOM Viewer 2023.1. For examiner reliability, measurements were made a second time by the same observer, one month apart.

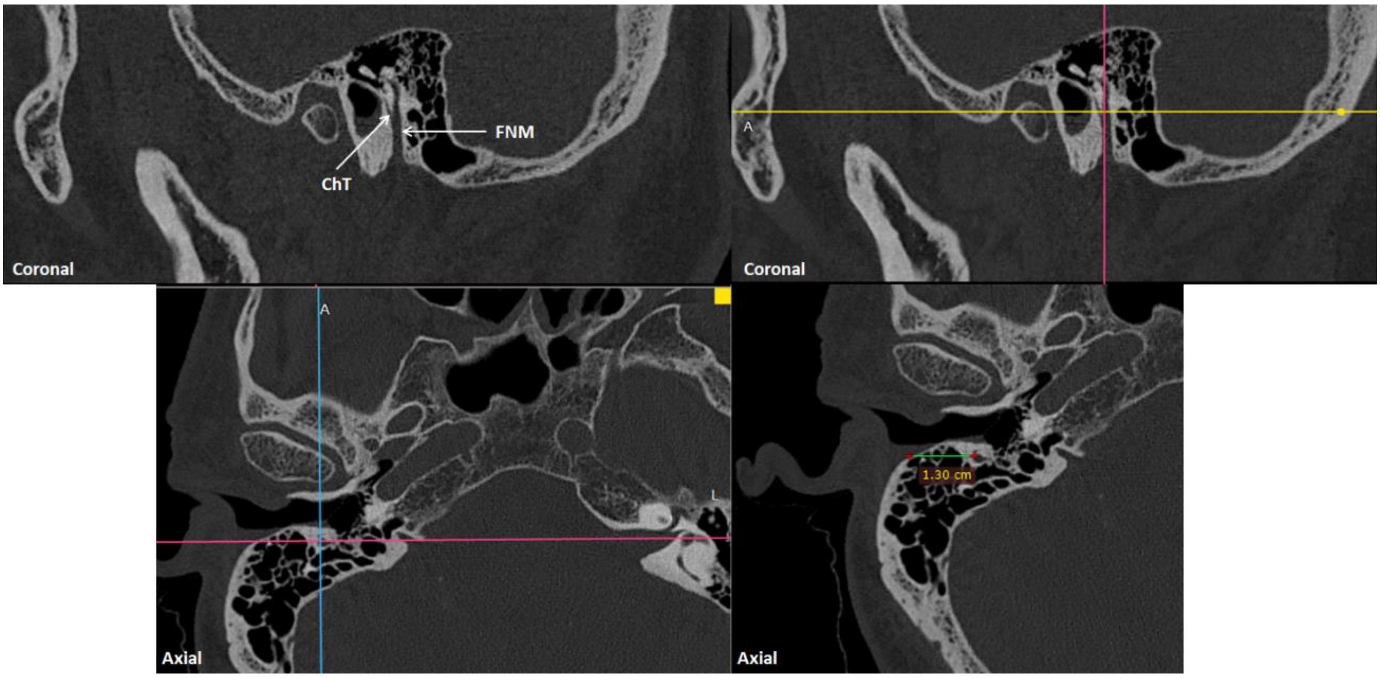

Figure 3.6 Measurement of the DFNM

FNM: Facial nerve mastoid segment, ChT: Chorda tympani

3.1.6. Calculation of the trajectory angles

After completed 3D reconstruction of the all anatomical structures (Figure 3.7a), the in-plane angle and out-plane angles have been calculated with OTOPLAN (Figure 3.7b).

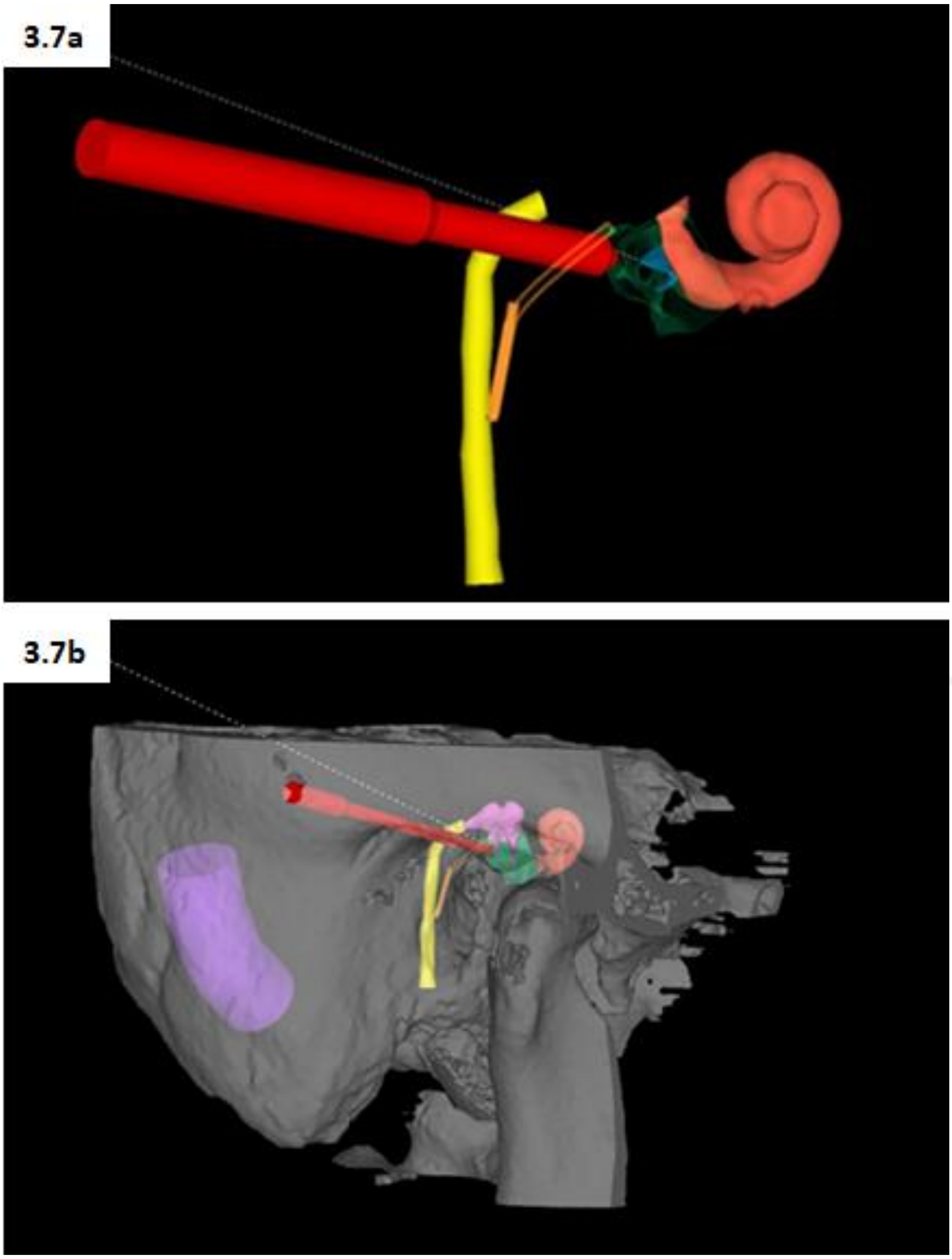

Figure 3.7 Calculation of the surgery trajectory angles

3.1.7. Calculation of the electrode insertion depth degree

Electrode insertion depth degree were calculated via OTOPLAN on postoperative CT images (Figure 3.8).

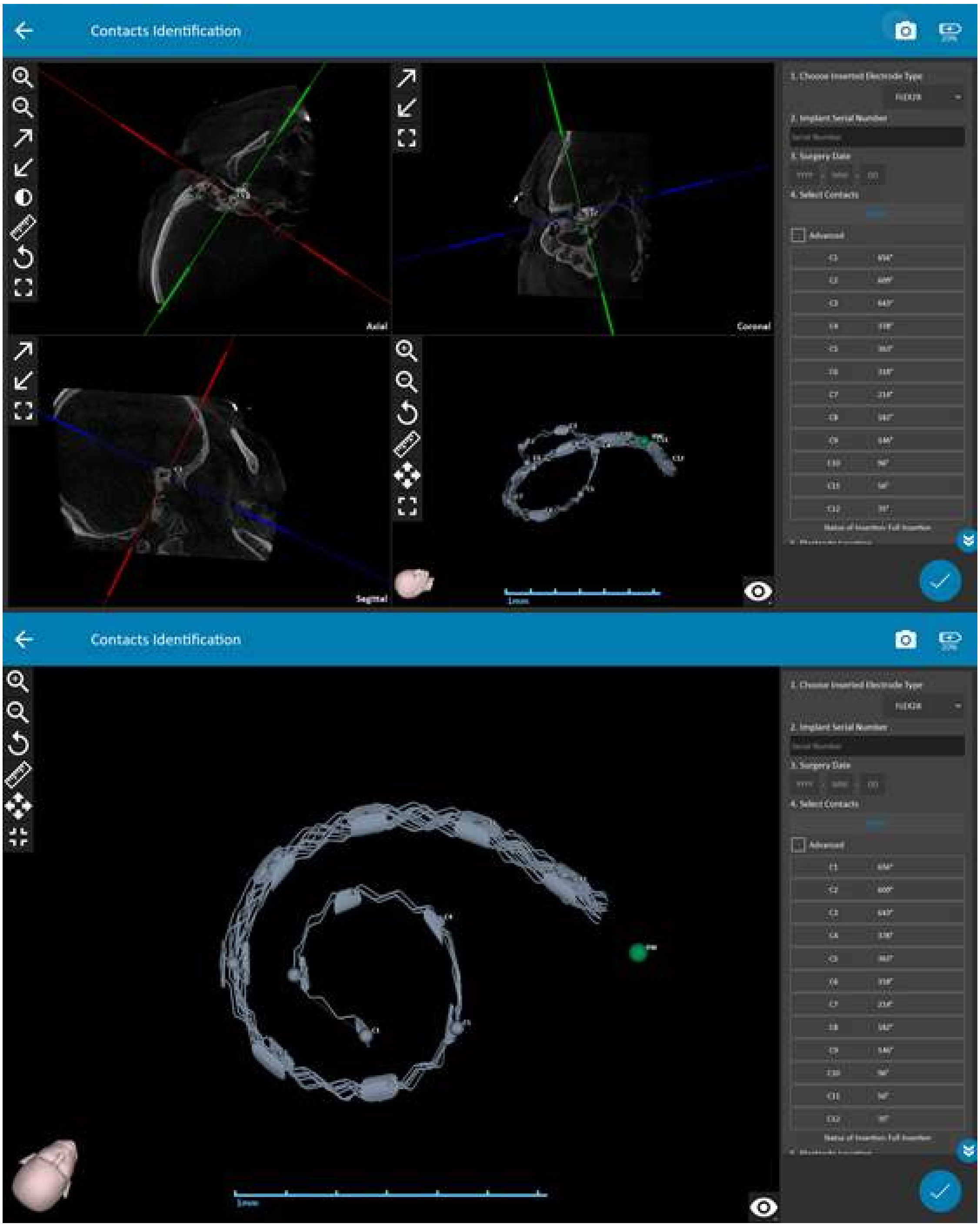

Figure 3.8 Calculation of electrode insertion depth degree

3.2. Statistical Method

Numerical data's adherence to the normal distribution was assessed using the Shapiro-Wilk test. To compare variables exhibiting a normal distribution between two groups, the Student's t-test was employed. The Mann-Whitney U test was utilized for comparing numerical variables that deviated from the normal distribution. The Pearson correlation coefficient was applied to examine relationships between numerical variables, while the chi-square test was employed for assessing relationships between categorical variables. The analysis was conducted using the SPSS 22.0 software package (IBM Corporation; Armonk, NY, USA). A significance level of $P<0.05$ was considered statistically significant.

4. RESULTS

4.1. Demographic Features of the Patients

CBCT images of 25 patients who underwent robot-assisted cochlear implant surgery (RACIS) and HRCT images of 33 patients who underwent conventional surgery (CS) were included in the study. No statistically significant difference was found between the patients who underwent RACIS and CS in terms of gender and age. Demographic features of patient who underwent cochlear implantation surgery are given in the Table 4.1.

Table 4.1 Demographic features of the patients

Surgery Group	RACIS	CS	P
Male	19, 76%	12, 36%	0.702
Female	6, 24%	21, 64%	0.587
Total	25	33	0.874
Age (Mean ± SD)	56.72±14.6	53.06±27.24	0.546

CS: Conventional surgery, RACIS: Robot-assisted cochlear implant surgery, SD: Standard deviation

4.2. The Results of the Anatomical Measurements of RACIS Patients

4.2.1. Cochlear sizes

The mean values of the cochlear sizes of the patients had RACIS are given in the Table 4.2.

Table 4.2 The mean cochlear sizes of the RACIS patients

Parameters	Total (25)	Male (19)	Female (6)	p
	(Mean±SD)	(Mean±SD)	(Mean±SD)	
Cochlear length (CL) (mm)	9.29±0.43	9.37±0.42	9.09±0.43	0.357
Cochlear width (CW) (mm)	6.74±0.48	6.84±0.38	6.48±0.63	0.130
Cochlear height (CH) (mm)	3.94±0.38	3.98±0.36	3.84±0.46	0.354
Cochlear duct length (CDL) (mm)	35.83±2.14	36.31±1.65	34.59±2.86	0.097
Basal turn length (BTL) (mm)	22.76±1.01	22.78±1.00	22.71±1.11	0.929

SD: Standard deviation

4.2.2. Round window and canonus measurements

The mean values of the round window and canonus measurements of the patients had RACIS are given in the Table 4.3. No statistical difference was detected between two canonus measurements taken one month apart (p=0.909).

Table 4.3 The mean round window and canonus sizes of the RACIS patients

Parameters		**Total (25)**	**Male (19)**	**Female (6)**	**p**
		(Mean±SD)	**(Mean±SD)**	**(Mean±SD)**	
Length of canonus (LC) (mm)		3.41±0.61	3.52±0.65	3.11±0.39	0.158
Thickness of canonus (TC) (mm)		1.29±0.41	1.24±0.40	1.43±0.43	0.220
Canonus type (Ct)	Flat	19	10	9	0.069
	Hook	6	3	3	
Superior-inferior distance of round window (RWSI) (mm)		1.88±0.37	1.95±0.31	1.71±0.49	0.198
Anterior-posterior distance of round window (RWAP) (mm)		1.60±0.49	1.70±0.48	1.36±0.45	0.244

SD: Standard deviation

Surgery was continued conventionally in 3 of 25 patients planned to be performed with RACIS due to intraoperative facial nerve monitoring (*In one patient, the software could not maintain a safe distance to the facial nerve (subject 19), and in the other two patients (subject 8 and 15), a software error occurred*). In the patient whose safe distance to the facial nerve could not be guaranteed with intraoperative imaging, the FRW, FRA and CAA, was statistically significantly lower than in other patients (p=0.021, p=0.03, p=0.005 respectively). The measurements of the 1 patient (*Subject 19*) who convert the conventional surgery and 22 patients who completed RACIS are given in the Table 4.4.

Table 4.4 Comparison between the 1 patient who the software could not maintain a safe distance to the facial nerve and 22 patients who completed RACIS

Parameters	Subject 19	RACIS (22)	P
CL (mm)	9.86	9.26±0.43	0.413
CW (mm)	7.05	6.71±0.48	0.725
CH (mm)	3.93	3.94±0.41	0.999
CDL (mm)	37.78	35.68±2.12	0.587
BTL (mm)	23.96	22.68±0.99	0.436
BTA (°)	64.40	59.31±8.50	0.238
CAA (°)	26.17	32.36±5.78	***0.005****
FRW (mm)	2.68	3.12±0.32	***0.021****
FRA (°)	29.31	39±6.55	***0.03****
DFNM (mm)	20.05	17.45±3.82	0.242
LC (mm)	3.36	3.42±0.63	0.793
TC (mm)	1.16	1.31±0.42	0.776
RWSI (mm)	2.05	1.87±0.39	0.816
RWAP (mm)	1.79	1.55±0.50	0.345

BTA: Basal turn angle, BTL: Basal turn length, CAA: Cochlea apical angle, CDL: Cochlear duct length, CH: Cochlear height, CL: Cochlear length, CW: Cochlear width, DFNM: Depth of the facial nerve mastoid segment, FRW: Facial recess width, FRA: Facial recess angle, LC: Length of canonus, RACIS: Robot-assisted cochlear implantation surgery, RWAP: Antero-posterior distance of round window, RWSI: Supero-inferior distance of round window, SD: Standard deviation, TC: Thickness of canonus

4.2.3. Cochlear orientation angles

The mean values of the cochlear orientation angles of the patients had RACIS are given in the Table 4.5. No statistical difference was detected between two measurements taken one month apart (p=0.947).

Table 4.5 The mean cochlear orientation angles of the RACIS patients

Parameters	Total (25) (Mean±SD)	Male (19) (Mean±SD)	Female (6) (Mean±SD)	p
Basal turn angle (BTA) (°)	58.72±8.49	58.98±9.49	58.05±5.70	0.923
Cochlea apical angle (CAA) (°)	33.04±7.02	33.61±7.99	31.60±3.57	0.423

SD: Standard deviation

4.2.4. Facial nerve measurements

The mean values of the facial nerve measurements of the patients had RACIS are given in the Table 4.6. No statistical difference was detected between two DFNM measurements taken one month apart (p=0.879).

Table 4.6 The mean facial nerve sizes of the RACIS patients

Parameters	Total (25) (Mean±SD)	Male (19) (Mean±SD)	Female (6) (Mean±SD)	p
Facial recess width (FRW) (mm)	3.01±0.48	3.15±0.51	2.98±0.33	0.235
Facial recess angle (FRA) (°)	34.04±5.88	34.11±6.12	33.86±5.66	0.976
Depth of FNM (DFNM) (mm)	17.60±3.79	18.04±4.26	16.47±1.98	0.164

SD: Standard deviation

4.2.5. The Trajectory Analysis of the RACIS Patients

In RACIS patients, the distance of the trajectory determined by 3D reconstruction to important anatomical points was calculated with OTOPLAN. In the patient whose safe distance to the facial nerve could not be guaranteed with intraoperative imaging (*Subject 19*), the distance between the planned trajectory and facial nerve was statistically significantly smaller than the other patients (p=0.033). The safety margin distances were given in the Table 4.7. The mean in-plane angle was 6.54±5.13, and the out-plane angle was 19.01±6.65.

Table 4.7 Safety margin distance

Groups	Subject 19	RACIS (22)	P
Stapes (mm)	1	1.08±0.45	0.254
Incus & Malleus (mm)	2.61	2.72±0.58	0.584
External auditory canal (mm)	1.53	1.53±0.65	0.369
Facial nerve (mm)	0.38	0.51±0.28	***0.033****
Chordae tympani (mm)	0.42	0.43±0.07	0.812

RACIS: Robotic assisted cochlear implantation surgery

Correlation Between the Trajectory Angles and Cochlear Sizes and Orientation

While a significant positive correlation was found between the basal turn angle and in plane angle (r=0.859, p=0.001), there was no significant correlation between other parameters (p>0.05).

4.3. The Results of the Anatomical Measurements of Conventional Cochlear Implantation Surgery Patients

4.3.1. Cochlear sizes

The mean values of the cochlear sizes of the patients had CS are given in the Table 4.8.

Table 4.8 The mean cochlear sizes of the CS patients

Parameters	Total	Male	Female	p
	Mean ± SD	**Mean ± SD**	**Mean ± SD**	
CL (mm)	9.69±0.98	9.91±1.15	9.49±0.81	0.068
CW (mm)	6.90±0.72	7.01±0.72	6.87±0.64	0.397
CH (mm)	3.36±0.48	3.43±0.35	3.41±0.36	0.601
CDL (mm)	37.00±3.53	37.73±3.86	36.49±3.36	0.571
BTL (mm)	23.52±2.36	24.09±2.80	23.07±1.96	0.068

BTL: Basal turn length, CDL: Cochlear duct length, CH: Cochlear height, CL: Cochlear length, SD: Standard deviation

4.3.2. Round window and canonus measurements

The mean values of the round window and canonus measurements of the patients had CS are given in the Table 4.9. No statistical difference was detected between two canonus measurements taken one month apart (p=0.967).

Table 4.9 The mean round window and canonus sizes of the CS patients

Parameters		Total	Male	Female	p
		Mean ± SD	Mean ± SD	Mean ± SD	
LC (mm)		2.84±0.61	2.92±0.34	2.82±0.65	0.182
TC (mm)		1.18±0.46	1.24±0.19	1.25±0.41	0.141
Ct	Flat	18	12	6	0.063
	Hook	15	10	5	
RWSI (mm)		2.00±0.25	1.92±0.33	1.89±0.30	0.762
RWAP (mm)		1.78±0.41	1.72±0.21	1.73±0.33	0.285

CT: Canonus type, LC: Length of canonus, RWAP: Antero-posterior distance of round window, RWSI: Supero-inferior distance of round window, SD: Standard deviation, TC: Thickness of canonus

4.3.3. Cochlear orientation angles

The mean values of the cochlear orientation angles of the patients had CS are given in the Table 4.10. No statistical difference was detected between two measurements taken one month apart (p=0.887).

Table 4.10 The mean cochlear orientation angles of the CS patients

Parameters	Total	Male	Female	p
	Mean ± SD	Mean ± SD	Mean ± SD	
BTA (°)	58.30±6.20	58.62±4.18	58.08±7.22	0.120
CAA (°)	30.12±4.89	29.07±5.14	30.67±4.71	0.543

BTA: Basal turn angle, CAA: Cochlea apical angle, SD: Standard deviation

4.3.4. Facial nerve measurements

The mean values of the facial nerve measurements of the patients had CS are given in the Table 4.11. No statistical difference was detected between two DFNM measurements taken one month apart (p=0.798).

Table 4.11 The mean facial nerve sizes of the CS patients

Parameters	**Total**	**Male**	**Female**	**p**
	Mean ± SD	**Mean ± SD**	**Mean ± SD**	
FRW (mm)	3.25±0.56	3.31±0.48	3.22±0.96	0.632
FRA (°)	31.58±5.74	31.94±6.09	31.41±5.60	0.844
DFNM (mm)	15.22±3.67	15.82±4.18	14.65±3.08	0.242

DFNM: Depth of the facial nerve mastoid segment, FRA: Facial recess angle, FRW: Facial recess width, SD: Standard deviation

4.4. Postoperative Electrode Insertion Depth Degree

The electrode insertion depth degree of 3 RACIS patients with cochlear ossification and anomalies (*Cogan syndrome, IP III, post-meningitis ossification*) was not included in the mean electrode insertion analysis. The postoperative electrode insertion depth degree of one of the RACIS patients could not be calculated because the postoperative CBCT images of one patient was suitable. Additionally, full electrode insertion was achieved in all patients except one RACIS patient. When comparing the anatomical measurements of this patient and other RACIS patients with full electrode insertion, the RWSI was significantly smaller in the patient with partial electrode insertion (1mm) than in the others (1.92±0.33 mm) (p=0.013).

The mean electrode insertion depth degree for the 18 RACIS patients and CS patients is given in table 4.12. There were no statistically significant differences between the CS and RACIS patients in insertion depth degree (p>0.05).

Table 4.12 Postoperative electrode insertion depth degree

Electrodes	Insertion depth degree (Mean ° ± SD)		P
	RACIS (18)	CS (33)	
C1	577±52	561±72	0.602
C2	506±65	501±69	0.911
C3	427±64	434±63	0.493
C4	357±49	372±62	0.233
C5	306±37	311±55	0.549
C6	262±32	258±54	0.881
C7	219±32	209±51	0.498
C8	176±30	161±50	0.231
C9	134±27	123±43	0.323
C10	94±26	88±37	0.511
C11	58±24	54±29	0.613
C12	28±16	29±22	0.677

CS: Conventional surgery, RACIS: Robotic assisted cochlear implantation surgery, SD: Standard deviation

4.4.1. Correlations Between the Anatomical Measurements and Postoperative Electrode Insertion in RACIS Patients

When the relationship between cochlear sizes and electrode insertion depth degrees was examined, a significant negative correlation was found between the basal turn length (BTL) and the last electrode (e12) insertion depth degree (p=0.007, r=0.545). Other sizes (CL, CW, CH, CDL) had no statistically significant effect on electrode insertion depth in degrees (p>0.05). There was no statistically significant relationship between BTA and CAA and postoperative electrode insertion depth degrees (p>0.05).

4.4.2. Correlations Between the Anatomical Measurements and Postoperative Electrode Insertion Depth Degree in CS Patients

When the relationship between cochlear sizes and electrode insertion depth degrees was examined, there was a significant negative correlation between BTL and CL and electrode insertion depth degree ($p=0.038$, $r=-0.363$). Other sizes (CW, CH, CDL) had no statistically significant effect on electrode insertion depth in degrees ($p>0.05$). In addition, a significant positive correlation was found between BTA and electrode insertion depth degree ($p=0.024$, $r=0.392$). There was no statistically significant relationship between CAA and postoperative electrode insertion depth degrees ($p>0.05$).

5. DISCUSSION

Particularly in the last 10 years, interest in robot-assisted cochlear implantation surgeries has increased. Accordingly, various studies have been conducted on the use of robots in CI surgeries (58). First, in 2014, Labadie et al. (73) showed that minimally invasive cochlear implantation was clinically feasible, however they encountered complications such as facial nerve injury and electrode trauma during surgery. In the current study, 3 of the 25 patients included were converted to conventional surgery due to facial nerve imaging. RACIS has made significant progress, especially with the advancement of image orientation technology. With RACIS, surgical intervention time is shortened, surgical intervention is standardized and tissue resection is reduced. This results in faster patient recovery and potentially faster hearing (3, 58). However, studies are still needed to prevent surgical complications, preserve residual hearing, and place electrodes with appropriate depth. To allow progress in robotic otological procedures a thorough analysis and knowledge of the temporal bone anatomy is necessaire, especially in the case of cochlear implantation that benefits from the cochlear tonotopy via electrode arrays. Surgical precision is worthless if there is not a thorough understanding of anatomy. Image guided surgery is paving fast forward the way for using anatomical knowledge in the clinical field more specifically CI. Still, there seems to be much unrevealed and the relevance of anatomical structures gains value if there is a technology that requires a study of them. Here we have studied the anatomy of the temporal bone in severe to profound patients who require cochlear implants. Our findings demonstrate that although the most accurate navigation and robot arm in healthcare is used, the anatomy still determines the difficulty or ease of RACIS.

5.1. Cochlear Dimensions

Before Mary Hardy (74) described cochlear duct length measurement with 68 specimens in 1938, Hensen in 1865, Waldeyer in 1873, Krause in 1876, and Retzius (75) in 1884 first reported cochlear duct measurements with smaller numbers of specimens (74). Since then, the human cochlea’s dimensions and morphology have been studied for years to identify variations between individuals. Since cochlear implants began to be used in the treatment of hearing loss, interest in knowing the dimensions of the cochlea has increased

(76). Jeffery and Spoor (77) reported that the cochlea reached adult dimensions at 17-19 weeks of gestation. Although the cochlea reaches its adult size during the fetal period, it differs significantly from person to person. Significant differences in cochlear dimensions between individuals have been reported (78-81). Accordingly, the need to design electrodes has become increasingly important to improve postoperative audiologic outcomes. Choosing the appropriate electrode for the patient is crucial to ensure proper cochlear coverage without placement trauma. Therefore, it is important to be able to predict the appropriate electrode and insertion depth preoperatively (76). In the literature, cochlea dimensions have been examined by different methods. These methods include direct method using a micrometer under a microscope from histological sections (74, 82-86), indirect method using histological sections and plastic molds (80, 87-90), 3D reconstruction software (79, 80, 91-94), cadaver temporal bones (74, 78), computed tomography, high-resolution computed tomography, micro-computed tomography and cone beam computed tomography images (29, 31, 69, 71, 72, 81, 95-103). In this study, cochlear dimensions were measured using OTOPLAN (CASCINATION AG, Bern, Switzerland), an otologic planning software. OTOPLAN enables the creation of patient-specific 3D reconstructions with tomography images. This facilitates accurate planning of cochlear intervention and is fully integrated into the HEARO system for robotic surgery. It has a powerful 3D modeling algorithm to visualize each patient's anatomy in full detail. It can also be easily used with a tablet or desktop computer (104).

The clinical term for the length of the cochlea is referred to as Distance A or the basal turn's diameter. Distance A represents the maximum measurement from the round window along the modiolar axis to the opposite wall. Clinically, Cochlear width is identified as Distance B, which is the measurement perpendicular to Distance A (29). In this study, the anatomical landmarks for cochlear length were the center point of the round window and the corresponding farthest point of the cochlea in coronal sections. In the literature, mean values for cochlear length were reported to range between 8.01 and 10.83 mm (74, 97). Cochlear width was reported between 5.73 mm and 8.71 mm in the literature (29, 103). The values found in this study are compatible with the literature. Cochlear height is the distance between the base of cochlea and the apex of the cochlea. In the literature, cochlear height values were reported between 1.43 mm and 6.81 mm (69, 79). The values found in the present study are compatible with the literature. Hardy (74) reported for the first time in 1938 that human cochlear canal length ranged between 25 mm and 35 mm in 68 cadaveric specimens. The mean cochlear canal length reported in the literature is between 28.4 mm and 42 mm (80, 89). A comparison of cochlear dimensions and the present study is given in Table 5.1 (27, 31, 69, 72, 78-80, 91-93, 101, 103, 105, 106).

van der Marel et al. (106) determined a negative correlation between length and width of cochlea and electrode insertion depth degree. Oh et al. (29) reported a negative correlation between both cochlear and basal turn length with final electrode insertion depth. Similarly, a negative correlation was found between cochlear length and basal turn length and final electrode depth in CS patients (p=0.038, r=-0.363). In robotic patients, there was a moderate negative correlation between basal turn length and depth of final electrode placement (p=0.007, r=-0.545).

Table 5.1 Comparison of cochlear dimensions reported in the literature and present study

Study	Method	CL (mm)	CW (mm)	CH (mm)	CDL (mm)	BTL (mm)
Retzius (1884) (75)	Histologic				33.5±0.8	
Hardy (1938) (74)	Histologic	10.83			31.52	
Bredberg (1968) (83)	Histologic				34±1.30	
Walby (1985) (88)	Histologic				32.6±2.1	
Uehlova et al. (1987) (82)	Histologic				34.2±2.9	
Pollak et al. (1987) (89)	Histologic				28.4±3.4	
Wright et al. (1987) (84)	Histologic				32.9±2.6	
Takagi and Sando (1989) (98)	Histologic				36.4	
Dimopoulos and Muren (1990) (78)	Plastic casts	8.58±0.45	6.77±0.35	3.93±0.40		
Sato et al. (1991) (95)	Histologic				34.73±2.9	
Kawano et al. (1996) (99)	Histologic				35.58±1.4	

Ketten et al. (1998) (79)	In vivo CT		7.91±0.53	1.43±0.26	33.01±2.31	-
Skinner et al. (2002) (97)	In vivo CT	8.01±0.30		1.56±0.22	34.62±1.2	
Sridhar et al. (2006) (85)	Histologic				33.31±2.4	
Escude et al. (2006) (72)	In vivo HRCT	9.23	6.99			
Stakhovskaya et al. (2007) (86)	Histologic				33.13±2.1	
Erixon et al. (2008) (80)	Plastic casts		6.8±0.46	3.9±0.37	42±1.96	
Lan et al. (2009) (103)	In vivo CT		8.71±0.29	4.79±0.45		
Lee et al. (2010) (90)	Histologic				30.8±0.6	
Martinez-Monedero et al. (2011) (27)	In vivo CT	8.62±0.49	6.55±0.47			
Erixon and Rask-Anderson (2013) (107)	Plastic casts	9.3±0.4			41.2±1.9	
Wimmer et al. (2013) (92)	In vivo µCT	9.35±0.32				
Shin et al. (2013) (93)	3D reconstruction	9.7±0.3	7±0.3	3.8±0.2	30±1.6	
Wurfel et al. (2014) (96)	In vivo CBCT				37.9±2.0	

van der Marel et al. (2014) (106)	In vivo CT	8.85±0.45	6.58±0.40			
Pelliccia et al. (2014) (69)	In vivo HRCT	9.12±0.68		6.81±0.50		
Meng et al. (2016) (81)	In vivo CT	9.04±0.31	6.33±0.28		35.8±2.00	21.1±1.1
Rivas et al. (2017) (91)	3D reconstruction	8.91 ± 0.49			32.71 ± 1.80	
Grover et al. (2018) (101)	In vivo HRCT	8.12			29.80	
Ketterer et al. (2018) (31)	In vivo HRCT	9.95±0.59	6.54±0.48	3.85±0.34		
Zahara et al. (2019) (105)	In vivo HRCT	8.75±0.31	6.53±0.35	3.26±0.24		
Oh et al. (2021) (29)	In vivo TBCT	8.67±0.42	5.73±0.32		36.20±1.57	21.07±1.01
Present study	In vivo CBCT	9.29±0.43	6.74±0.48	3.94±0.38	35.83±2.14	22.76±1.01
	In vivo HRCT	9.69±0.98	6.90±0.72	3.36±0.48	37.00±3.53	23.52±2.36

BTL: Basal turn length, CBCT: Cone-beam computed tomography, CDL: Cochlear duct length, CH: Cochlear height, CL: Cochlear length, CT: Computed tomography, CW: Cochlear width, HRCT: High resolution computed tomography, TBCT: Temporal bone computed tomography, µCT: Micro computed tomography

5.2. Cochlear Orientations

The alignment of the cochlea at the cranial base is determined by the angle between the basal turn of the cochlea and the mid-sagittal line of the skull, as indicated by previous research (27, 108). This angle is also defined as the basal turn angle (108). It has been observed through studies that the orientation of the cochlea undergoes changes during the initial years of life (27, 108). The cochlea reaches adult size with ossification of the otic capsule at approximately 17-19 weeks of gestation. On the contrary, the development of the skull base and the petrous part of the temporal bone surrounding the cochlea persists. This development is not linear and also differs between the sexes. Rapid skull growth occurs between the ages of 1 and 4, as well as between 11 and 12 years. This is followed by the completion of the spheno-occipital synchondrosis (108). The postnatal change of the skull base also changes the orientation of the cochlea at the skull base (27). Lloyd et al. (108) found that the mean basal turn angle in adults was 54.6. They also reported that BTA decreased with age (108). Martinez Monedero et al. (27) found the mean adult value of BTA to be 57.82±3.75. Similarly, it was reported that BTA decreased with increasing age (27).

BTA is is a crucial parameter that significantly influences the accessibility to the cochlear basal turn. Lloyd et al. (108) reported that a larger BTA causes a difficult cochlear implantation. In this study, the relationship between BTA and surgical approach angles was analyzed and a very strong positive correlation was found between BTA and in-plane angle ($r=0.859$, $p=0.001$). As far as our knowledge extends, this study represents the initial attempt to statistically analyze the correlation between cochlear orientation and surgical approach angles. Our results suggest that a large CTA may complicate the ideal surgical approach.

Cochlea apical angle is the angle between the long axis of the cochlea and the midsagittal axis. In our study, the mean cochlea apical angle value was 33.04 ± 7.02 in RACIS patients and 30.12 ± 4.89 in CS patients. Unlike the basal turn angle, there was no significant correlation between the cochlea apical angle value and the surgical approach angles.

5.3. Facial Recess Sizes

To mitigate the risk of facial nerve damage in cochlear implantation surgery, the MPTA remain the established gold standard, although different modalities such as suprameatal and pericanal approaches have been offered as alternatives to the posterior tympanotomy approach (109, 110). The two most important complications of cochlear implantation surgery with MPTA are facial paralysis and taste disturbances due to facial nerve and chorda tympani damage (111). Therefore, both access to the cochlea and the risk of facial nerve and chorda tympani damage are significantly affected by the facial recess width during cochlear implantation surgery (112). The facial recess is the area situated between the mastoid segment of the facial nerve, the tympanic annulus, and the chorda tympani. The dimensions of the facial recess undergo alterations during fetal development, influenced by the maturation of the facial canal and fibrous annulus. Studies indicate that in term babies, the width of the facial recess is around 3.25 mm at the level of the oval window and 2.62 mm at the level of the round window. These measurements increase with age, reaching approximately 3.79 mm and 3.04 mm, respectively (113). In MPTA, the round window is reached from the facial recess with a high-speed drill (3, 112). Accessing the ST through the RW has some advantages over cochleostomy (114, 115). However, access to the RW through the facial recess approach may not be easy in all cases. In this case, facial recess anatomy becomes more important. Facial recess anatomy has been studied with various methods due to its clinical importance (111, 112, 116-129). In the present study, 3D reconstruction of the facial canal and ChT was performed with HRCT and CBCT images. The software automatically calculated the facial recess width according to the planned trajectory towards the RW.

In the literature, the mean width of the FR has been reported as 0.7 mm to 4.5 mm (112, 113). In the current study, the mean FRW of RACIS patients and CS patients were 3.01±0.48 and 3.25±0.56, respectively. Wang et al. (113) found that 39 patients with narrow FR had a FRW in the range of 0.7 mm-1 mm. In another study, the mean FRW of patients with narrow FR was 0.85 mm (130). Narrow FR is usually caused by ChT variations and these patients are at increased risk of damage to the FN or ChT during cochlear implantation. In the present study, there were no patients with a facial recess size less than 1mm; however, in the 1 patients whose safe distance to the facial nerve could not be guaranteed with intraoperative imaging, the facial recess width and facial recess angle was significantly smaller than in other patients (p=0.021 and p=0.03). In addition, the distance of the surgical trajectories to the facial nerve was significantly smaller in the 1 patient whose safe distance to the facial nerve could not be guaranteed with intraoperative imaging than in the other patients (p=0.033). A comparison of facial recess size and facial recess angle values reported in the literature with the current study is given in Table 5.2.

Table 5.2 Comparison of facial recess sizes reported in the literature and present study

Study	Method	FRW (mm)	FRA (°)
Su et al. (1982) (116)	Dry bone	4.01 ± 0.56	
Bielamowicz et al. (1988) (117)	Dry bone	2.65 ± 0.63	
Young and Nadol (1989) (118)	Dry bone	3.01 ± 0.58	
Bettman et al. (2003) (112)	CT	4.5 ± 1.3	
Zhu Y et al. (2008) (122)	Cadaveric temporal bone		24.8
Calli et al. (2010) (123)	Cadaveric temporal bone		23.58 ± 6.84
Maru N et al. (2010) (124)	Cadaveric temporal bone		26 - 35
Zou et al (2012) (127)	Cadaveric temporal bone	2.73 ± 0.20	
Jeon et al. (2013) (125)	CT		18.40 ± 1.05
Wang et al. (2013) (128)	Cadaveric temporal bone	2.94 ± 0.32	
Wang et al. (2013) (113)	In vivo	0.7-1	
Kashia et al. (2014) (129)	CT	4.4 ± 0.8	
Wang et al. (2015) (130)	In vivo	0.85	
Diogo I et al. (2016) (126)	CBCT		22.6 ± 9.5
Jain et al. (2018) (120)	Cadaveric temporal bone	2.93 ± 0.4	26.90 ± 1.19
Present study	In vivo CBCT	3.01 ± 0.48	34.04 ± 5.88
	In vivo HRCT	3.25 ± 0.56	31.58 ± 5.74

CBCT: Cone-beam computed tomography, HRCT: High resolution computed tomography, FRA: Facial recess angle, FRW: Facial recess width

In addition to these, the distance of the facial nerve (FN) to the mastoid surface, i.e., the depth of the FN within the temporal bone, is crucial in both robotic and conventional surgery. However, literature on findings related to the depth of the FN is quite limited. Aslan et al. (12), reported that in 90 HRCT images, the FN was 15 mm medial to the mastoid surface. Dai et al. (131) reported that the mean distance was 19.07 mm between the lateral edge of the mastoid process and the central point of the FN. They also mentioned that the FN is more laterally positioned in males compared to females (131). Additionally, it is noted that the position of the FN in the temporal bone is influenced by mastoid pneumatization (12, 131). In the current study, the mean DFNM in RACIS patients was 17.60 ± 3.79, and 15.22 ± 3.67 in the CS patients.

5.4. Round window and canonus

Round window (RW) was initially described by Antonio Scarpa in 1772 (132). It is situated on the medial wall of the tympanic cavity, positioned at the termination of the ST facing the tympanic cavity (116). The medial wall of the RW is formed by the subiculum, while its superior and lateral walls are shaped by the promontory (42, 116). The RW is covered by a membrane called secondary tympanic or round window membrane (35, 36, 132, 133). Scarpa, who was also the first to discover the round window membrane, reported that RW appeared in a single plane.

In cochlear implantation surgery, access to the cochlea is provided via cochleostomy or round window (7, 133). The continuity of the RW with the ST ensures safe placement of electrodes in this compartment (134). Todt et al. (115) reported that the functional integrity of the vestibular receptors was more preserved in the RW approach in their study comparing cochleostomy and round window. Gudis et al. (114) reported that the facial recess approach followed by electrode placement through the round window was safer and more effective. In the light of these data, while the RW approach is deemed the most optimal for cochlear implant surgery, it is crucial to exercise care to avoid harm to the spiral ligament, basilar membrane, and osseous spiral lamina during the procedure (7). Because of its clinical importance and variable anatomy, the round window has been analyzed with various methods in the literature (16, 17, 116, 133, 135-140). In surgical approaches to the RW, it is essential to know the anatomic variations, morphologic and morphometric features of the RW (16). The comparison of RW dimensions reported in the literature with the present study is given in Table 5.3. It has been reported that electrode placement through the RW may be difficult when the height and width of the RW are <1 mm (137). In the current study, complete placement could not be achieved in one of the RACIS patients and the RW supero-inferior diameter (1 mm) of the patient who could not achieve complete placement was found to be significantly lower than the others (p=0.013).

The promontory hangs down from the RW in the form of a bony ridge. This ridge includes an anterior pillar (*postis anterior*), a tegmen and a posterior pillar (*postis posterior*). In recent studies, the term canonus has been proposed for the canopy bony prominence that partially covers and protects the RW (42). The anatomical features of the canonus are important for cochlear implantation (135, 141). According to our current knowledge no study is reporting morphometric and morphological analysis of canonus in the literature. In the present study, the mean canonus thickness has been founded 1.29±0.41 mm in RACIS patients and 1.18±0.46 in CS patients. Mean canonus length was 1.56±0.11 in RACIS patients and 1.74±0.30 in conventional patients. In the HEARO procedure, the canonus is milled with a 1.0-mm tungsten carbide diamond burr (canonostomy) (3). Therefore, the canonus thickness should be known in advance. The canonus was also categorized as hook and flat according to its shape. Since RW seemed more difficult in hook type compared to flat type, this classification may be significant in the surgery.

Table 5.3 Comparison of round window sizes reported in the literature and present study

Study	Method	RWSI (mm)	RWAP (mm)
Stewart and Belal (1981) (140)	Cadaver	1.2	1.5
Su et al. (1982) (116)	Dry bone	1.66 ± 0.34	
Takahashi et al. (1989) (143)	Dry bone CT	2.08±0.22	1.76±0.10
Bonaldi et al. (1997) (133)	Fetus	1.74 ± 0.35	1.22 ± 0.21
Cohen et al. (2005) (136)	In vivo CT	1.66 ± 0.25	
Atturo et al. (2014) (16)	Dry bone	1.90±0.26	1.54±0.29
Singla et al. (2014) (137)	Dry bone	1.62±0.77	1.15±0.39
Chen et al. (2015) (139)	In vivo CT	2.47 ± 0.35	1.81 ± 0.45
Seliet et al. (2018) (138)	Dry bone	1.91±0.78	1.37±0.43
Vayisoglu et al. (2021) (17)	Fetus	1.48 ± 0.25	1.57 ± 0.37
Present study	In vivo CBCT	1.88±0.37	1.60±0.49
	In vivo HRCT	2.00±0.25	1.78±0.41

CT: Computed tomography, CBCT: Cone-beam computed tomography, HRCT: High resolution computed tomography

5.5. Trajectory angles

During robot-assisted cochlear implant surgery, a minimally invasive pathway to the cochlea is established through a small tunnel that opens from the mastoid surface, traversing the facial recess to reach the cochlea (26, 42). In addition to minimally invasive access, it is important not to damage intracochlear structures and preserve residual hearing during electrode placement. For this reason, the ideal placement trajectory in the ST should be aligned with the center line of the ST to avoid damage to the basilar membrane, modiolus and spiral ligament during placement (21, 26, 65). Tores et al. (143), reported a significant association between insertion axes that were not close to the ideal insertion angle and intracochlear trauma. Aebischer et al. (21) found a mean in-plane angle of 18°±13° for a given target, defined as the deviation between the planned trajectory and the ideal trajectory relative to the basal rotation of the cochlea. In addition, he reported a mean out-plane angle of 10°±11°, defined as the deviation between the planned and calculated ideal trajectory at basal rotation in a perpendicular plane (21). In the present study, the mean in-plane angle was 6.54°±5.13°, and the out-plane angle was 19.01°±6.65°. In addition, there was significant positive correlation between the basal turn angle and in plane angle (r=0.859, p=0.001). A previous study reported that a larger basal turn angle caused a difficult cochlear implantation (108). Although surgical approach angles have been previously investigated in experimental and in-vitro studies, to the best of our knowledge, this is the first time that the relationship between cochlear orientation and surgical approach angles has been statistically compared. In conclusion, it may be due to this relationship with in-plane angle that a large BTA may cause difficult cochlear implantation.

5.6. Electrode insertion

The process of electrode placement plays a pivotal role in cochlear implant surgery. The success of the cochlear implant is contingent upon the complete insertion of the electrode array into the scala tympani without any deviation (2, 58). Although electrode insertion in the HEARO procedure is still performed manually by the surgeon, tele-manipulators are available that allow the electrode array to be placed in the inner ear at a certain speed and in a standardized manner (67, 68). Daoudi et al. (144) found more electrode scalar deviation in 40 CI patients with manual insertion than in 20 CI patients with robotic insertion. In the present study, electrode insertion was performed manually in both conventional and robotic patients. Complete insertion was not achieved in only one of the RACIS patients. In this patient, the round window supero-inferior distance was 1 mm, which was statistically significantly smaller than the other patients (p=0.013). Singla et al. (137) reported that electrode insertion through the RW may be difficult when the RW height and width are <1 mm. Johnston et al. (145) found that cochlear length (distance A) was significantly greater in the patient group with complete insertion than in the group without complete insertion. In the current study, patient with incomplete insertion did not exhibit any significant differences in other parameters, except for RWSI, when compared to those with complete insertion.

In addition to full insertion, electrode type and angular insertion depth also significantly affect postoperative clinical outcomes (146). Preoperative prediction of angular insertion depth is essential for the surgical plan. Several studies have shown that deeper insertion angle is is correlated with improved speech performance, primarily attributed to enhanced stimulation of the apical region (147-150). Cochlea dimensions significantly affect the insertion depth. In addition, there is a need for electrode selection according to variable cochlea dimensions (29). Oh et al. (29) found a significant negative correlation of distance A and B with insertion depth degree. Similarly, van Der Marek et al. (106) reported a negative correlation between insertion depth and cochlear diameters. Franke-Trieger et al. (70) found the significant negative correlation between insertion depth degree and the BTL. In the present study, there was significant negative correlation between basal turn length and final electrode insertion depth in RACIS patients (p=0.007, r=-0.545). In the conventional group, there was a statistically significant negative correlation between basal turn lenght and cochlear length and electrode insertion depth degree (p=0.038, r=-0.363).

5.7 Comparison the RACIS and MPTA

The gold standard for CI surgery is a large cortical mastoidectomy and a wide posterior tympanotomy. Postelmans (151) reported that the incidence of facial nerve palsy in posterior tympanotomy is 0.5-2%. To eliminate the risk of damage to the facial nerve during CI surgery, alternating approaches away from the facial nerve have been proposed (153). Suprameatal and pericanal approaches are examples of these alternative methods. However, there are still concerns about the appropriate angle of access to the cochlea with these methods. Because the appropriate approach angle to the cochlea may significantly affect hearing outcomes (10). In addition, contact of the electrode array with the bone chain in the suprameatal approach may cause conductive hearing loss. Both techniques require raising the tympanic membrane and opening the middle ear, which increases the risk of damage to the tympanic membrane (10). For all these reasons, MPTA is clearly the most ideal approach among conventional methods compared to other methods.

When a direct access keyhole trajectory with ideal cochlear approach angles is applied, angular deviations from the planned trajectory are on the order of microns (10). Deviations at this level require extraordinary human skill. For this reason, robotic cochlear implantation trials have increased in recent years. In 2017, Weber et al. (5) first performed keyhole posterior tympanatomy in 6 patients with a robotic arm they developed. In 2019, Caversicco et al. (60) performed robotic middle ear access in 6 patients.

Although electrode placement in robotic CI is still performed manually, Schneider et al. (62) successfully performed electrode placement through a drilled tunnel in 4 ex vivo human head specimens. Similarly, Kaufman et al. (68) completed robot-assisted electrode placement in fresh frozen human cadaveric cochlea.

Software glitches in robotic surgery, poor image quality, and a certain routine for doctors and nurses may cause the operation time to be longer than normal. However, robotic surgery may allow less invasive surgery with the development of smaller tunnels for smaller electrodes. It also allows for greater preservation of residual hearing.

In the present study, RACIS patients whose surgical trajectories were anatomically analyzed were operated with the HEARO procedure (3). Additionally, 33 patients were operated on with MPTA by the same surgeon. The electrode used in both groups was the same (Med-el Flex 28) and there was no significant difference in the electrode insertion depth angle between the groups (Table 4.12). In the HEARO group, although access to the inner ear was completely robotic, electrode placement was performed manually. Only one of these patients had no contact at the last electrode. Daoudi et al. (144) reported robot-assisted electrode placement using RobOtol® following conventional mastoidectomy. Comparing manual placement with robot-assisted placement, they reported that robotic placement was less traumatic than manual placement (144). This stage is still accomplished manually by the surgeon in the HEARO procedure (3, 58). Despite this, the RobOtol® and iotaSOFT® systems can ensure that an electrode is placed at a given speed (67, 68). However, none of these yet guarantee a standard insertion into the inner ear with a right angle (58).

6. CONCLUSION

In this thesis, anatomical parameters that could affect the safe trajectory in robotic cochlear implantation surgery were identified. It was observed that the width of the facial recess and the angle of the facial recess are critical factors for a safe trajectory. According to our current knowledge, studies evaluating the relationship between cochlear orientation and surgical trajectory angles are very limited in the literature. The results of this study showed that cochlear orientation can influence surgical approach angles. Therefore, preoperative evaluation of cochlear orientation is essential for safe cochlear access.

Additionally, electrode insertion depth degrees were evaluated with postoperative CT images. As expected, there was a negative correlation between basal turn length and the final electrode insertion depth degree in both RACIS and CS cases. Moreover, in CS cases, cochlear length also negatively affected the final electrode insertion depth degree. Thus, in both robotic and conventional surgery, preoperative assessment of cochlear dimensions is crucial for appropriate electrode selection and, consequently, for postoperative audiological outcomes.

In a case where complete insertion could not be achieved, the identification of a significantly small round window suggests that a small round window may hinder full electrode insertion.

The findings of this study are considered to be a reference for future studies in achieving collision-free trajectory planning in robotic-assisted cochlear implant surgery.

7. REFERENCES

1. Smith RJ, Bale Jr JF, White KR. Sensorineural hearing loss in children. Lancet. 2005;365(9462):879-890.

2. Van de Heyning P, Roland P, Lassaletta L, Agrawal S, Atlas M, Baumgartner WD, et al. Suitable Electrode Choice for Robotic-Assisted Cochlear Implant Surgery: A Systematic Literature Review of Manual Electrode Insertion Adverse Events. Front Surg. 2022;9:823219.

3. Topsakal V, Heuninck E, Matulic M, Tekin AM, Mertens G, Van Rompaey V, et al. First Study in Men Evaluating a Surgical Robotic Tool Providing Autonomous Inner Ear Access for Cochlear Implantation. Front Neurol. 2022;13:804507.

4. Rubinstein JT. Paediatric cochlear implantation: prosthetic hearing and language development. Lancet. 2002;360(9331):483-485.

5. Weber S, Gavaghan K, Wimmer W, Williamson T, Gerber N, Anso J, et al. Instrument flight to the inner ear. Sci Robot. 2017;2(4):eaal4916.

6. Cochlear Implants, https://www.nidcd.nih.gov/health/cochlear-implants#:~:text=Children%20and%20adults%20who%20are,adults%20and%2065%2C000%20in%20children., Accessing date: 29.06.2023.

7. DeSaSouza S. Cochlear Implants: New and Future Directions. Springer Nature Singapore, 2022.

8. Praetorius M, Staecker H, Plinkert P. Surgical technique in cochlear implantation. HNO. 2009;57(7):663-670.

9. Carlson ML. Cochlear implantation in adults. N Engl J Med. 2020;382(16):1531-1542.

10. Topsakal V, Matulic M, Assadi MZ, Mertens G, Rompaey VV, Van de Heyning P. Comparison of the Surgical Techniques and Robotic Techniques for Cochlear

Implantation in Terms of the Trajectories Toward the Inner Ear. J Int Adv Otol. 2020;16(1):3-7.

11. Ulug T. Atlas of Temporal Bone Surgery. New York: Thieme, 2011: s.15-33.

12. Aslan A, Göktan C, Okumus M, Tarhan S, Unlu H. Morphometric analysis of anatomical relationships of the facial nerve for mastoid surgery. J Laryngol Otol. 2001;115:447-449.

13. Gantz BJ. Intraoperative facial nerve monitoring. Am J Otol. 1985;6:58-61.

14. Hsieh H-S, Wu C-M, Zhuo M-Y, Yang C-H, Hwang C-F. Intraoperative facial nerve monitoring during cochlear implant surgery: an observational study. Medicine (Baltimore). 2015;94(4).

15. HEARO-The World's First Robot for Cochlear Implantation, https://www.cascination.com/en/hearo#:~:text=The%20HEARO%20robotic%20system%20enables,mm%20from%20the%20facial%20nerve. Accessing date: 29.06.2023

16. Atturo F, Barbara M, Rask-Andersen H. Is the human round window really round? An anatomic study with surgical implications. Otol Neurotol. 2014;35(8):1354-1360.

17. Vayisoğlu Y, Beger O, Güven O, Adanır SS, Taghipour P, Çakır S, et al. Anatomic features of the fetal round and oval windows, and their relations with the tympanic nerve. Surg Radiol Anat. 2021;43(7):1203-1221.

18. Panara K, Shahal D, Mittal R, Eshraghi AA. Robotics for Cochlear Implantation Surgery: Challenges and Opportunities. Otol Neurotol. 2021;42(7):e825-e835.

19. Ansó J, Scheidegger O, Wimmer W, Gavaghan K, Gerber N, Schneider D, et al. Neuromonitoring during robotic cochlear implantation: initial clinical experience. Ann Biomed Eng. 2018;46(10):1568-1581.

20. Caversaccio M, Gavaghan K, Wimmer W, Williamson T, Ansò J, Mantokoudis G, et al. Robotic cochlear implantation: surgical procedure and first clinical experience. Acta Otolaryngol. 2017;137(4):447-454.

21. Aebischer P, Mantokoudis G, Weder S, Anschuetz L, Caversaccio M, Wimmer W. In-Vitro Study of Speed and Alignment Angle in Cochlear Implant Electrode Array Insertions. IEEE Trans Biomed Eng. 2022;69(1):129-137.

22. Jiam NT, Limb CJ. The impact of round window vs cochleostomy surgical approaches on interscalar excursions in the cochlea: Preliminary results from a flat-panel computed tomography study. World J Otorhinolaryngol Head Neck Surg. 2016;2(03):142-147.

23. Nguyen Y, Miroir M, Kazmitcheff G, Sutter J, Bensidhoum M, Ferrary E, et al. Cochlear implant insertion forces in microdissected human cochlea to evaluate a prototype array. Audiol Neurootol. 2012;17(5):290-298.

24. Roland Jr JT. A model for cochlear implant electrode insertion and force evaluation: results with a new electrode design and insertion technique. Laryngoscope. 2005;115(8):1325-1339.

25. Wimmer W, Bell B, Huth ME, Weisstanner C, Gerber N, Kompis M, et al. Cone beam and micro-computed tomography validation of manual array insertion for minimally invasive cochlear implantation. Audiol Neurootol. 2014;19(1):22-30.

26. Wimmer W, Venail F, Williamson T, Akkari M, Gerber N, Weber S, et al. Semiautomatic cochleostomy target and insertion trajectory planning for minimally invasive cochlear implantation. Biomed Res Int. 2014;2014:596498.

27. Martinez-Monedero R, Niparko JK, Aygun N. Cochlear coiling pattern and orientation differences in cochlear implant candidates. Otol Neurotol. 2011;32(7):1086-1093.

28. Pietsch M, Schurzig D, Salcher R, Warnecke A, Erfurt P, Lenarz T, et al.Variations in Microanatomy of the Human Modiolus: Implications for Cochlear Implants. Scientific Reports. 2021.

29. Oh J, Cheon JE, Park J, Choi YH, Cho YJ, Lee S, et al. Cochlear duct length and cochlear distance on preoperative CT: imaging markers for estimating insertion depth angle of cochlear implant electrode. Eur Radiol. 2021;31(3):1260-1267.

30. Morrel WG, Holder JT, Dawant BM, Noble JH, Labadie RF. Effect of scala tympani height on insertion depth of straight cochlear implant electrodes. Otolaryngol Head Neck Surg. 2020;162(5):718-724.

31. Ketterer MC, Aschendorff A, Arndt S, Hassepass F, Wesarg T, Laszig R, et al. The influence of cochlear morphology on the final electrode array position. Eur Arch Otorhinolaryngol. 2018;275(2):385-394.

32. Büchner A, Illg A, Majdani O, Lenarz T. Investigation of the effect of cochlear implant electrode length on speech comprehension in quiet and noise compared with the results with users of electro-acoustic-stimulation, a retrospective analysis. PLoS One. 2017;12(5):e0174900.

33. Jagt A, Kalkman RK, Briaire JJ, Verbist BM, Frijns JH. Variations in cochlear duct shape revealed on clinical CT images with an automatic tracing method. Sci Rep. 2017;7(1):1-9.

34. Moore KL, Persaud TVN, Torchia MG. The Developing Human: Clinically Oriented Embryology. 10 baskı. USA: Elsevier, 2016: s.428-435.

35. Presutti L, Marchioni D. Endoscopic ear surgery principles, indications, and techniques. New York: Thieme, 2014: s.49-52.

36. Standring S. Gray's Anatomy: The Anatomical Basis of Clinical Practice. 41 baskı.: Elsevier Limited, 2016: s.628-650.

37. Swartz JD, Loevner LA. Imaging of the Temporal Bone. 4 baskı. New York: Thieme, 2011: s.444-460.

38. Moore KL, Agur AMR, Dalley AF. Clinically Oriented Anatomy. Wolters Kluwer Health, 2018: s.2183-2197.

39. Phillips CD, Bubash LA. The facial nerve: anatomy and common pathology. Semin Ultrasound CT MR. 2002;23(3):202-217.

40. Seneviratne SO, Patel BC. Facial nerve anatomy and clinical applications. StatPearls2023.

41. Gordin E, Lee TS, Ducic Y, Arnaoutakis D. Facial nerve trauma: evaluation and considerations in management. Craniomaxillofac Trauma Reconstr. 2015;8(1):1-13.

42. Topsakal V, Kachlik D, Bahşi I, Carlson M, Isaacson B, Broman J, et al. Relevant temporal bone anatomy for robotic cochlear implantation: An updated terminology combined with anatomical and clinical terms. Translational Research in Anatomy. 2021;25:100138.

43. Corrales CE, Mudry A. History of the Endolymphatic Sac: From Anatomy to Surgery. Otol Neurotol. 2017;38(1):152-156.

44. Hall JE, Hall ME. Guyton and Hall Textbook of Medical Physiology: Guyton and Hall Textbook of Medical Physiology E-Book. Elsevier Health Sciences, 2020.

45. Roux A-F, Pallares-Ruiz N, Vielle A, Faugère V, Templin C, Leprevost D, et al. Molecular epidemiology of DFNB1 deafness in France. BMC Med Genet. 2004;5(1):1-10.

46. Bayazıt YA, Cable BB, Cataloluk O, Kara C, Chamberlin P, Smith RJ, et al. GJB2 gene mutations causing familial hereditary deafness in Turkey. Int J Pediatr Otorhinolaryngol. 2003;67(12):1331-1335.

47. Pandya A, Arnos KS, Xia XJ, Welch KO, Blanton SH, Friedman TB, et al. Frequency and distribution of GJB2 (connexin 26) and GJB6 (connexin 30) mutations in a large North American repository of deaf probands. Genet Med. 2003;5(4):295-303.

48. Liu Y, Ke X, Qi Y, Li W, Zhu P. Connexin26 gene (GJB2): prevalence of mutations in the Chinese population. J Hum Genet. 2002;47(12):688-690.

49. Dahl E, Manthey D, Chen Y, Schwarz H-J, Chang YS, Lalley PA, et al. Molecular cloning and functional expression of mouse connexin-30, a gap junction gene highly expressed in adult brain and skin. J Biol Chem. 1996;271(30):17903-17910.

50. del Castillo I, Villamar M, Moreno-Pelayo MA, del Castillo FJ, Álvarez A, Tellería D, et al. A deletion involving the connexin 30 gene in nonsyndromic hearing impairment. N Engl J Med. 2002;346(4):243-249.

51. Koomen I, Grobbee DE, Roord JJ, Donders R, Jennekens-Schinkel A, Van Furth A. Hearing loss at school age in survivors of bacterial meningitis: assessment, incidence, and prediction. Pediatrics. 2003;112(5):1049-1053.

52. Michels TC, Duffy MT, Rogers DJ. Hearing loss in adults: differential diagnosis and treatment. Am Fam Physician. 2019;100(2):98-108.

53. Volta A. On the electricity excited by the mere contact of conducting substances of different kinds. Philos Trans R Soc. 1800;90:403-431.

54. Luxford W, Brackmann D. The history of cochlear implants. RF G (Editör). Cochlear implants. London: Croom Helm, 1985: s.1-26.

55. Andreef AM GG, Volokhov AA. Electrical stimulation of the hearing organ. J Physiol USSR. 1934;1:546-549.

56. Yoshimura H, Moteki H, Nishio S-y, Usami S-i. Electric-acoustic stimulation with longer electrodes for potential deterioration in low-frequency hearing. Acta Otolaryngol. 2020;140(8):624-630.

57. Black B. Keyhole cochlear implantation: current status. Otol Neurotol. 2011;32(9):1459-1463.

58. Abari J, Tekin A, Topsakal V. Robot-Assisted Cochlear Implant Surgery. 2023.

59. Wimmer W, Weber S, Anso J, Gerber K, Rathgeb C, Mantokoudis G, et al. Robotic cochlear implantation: first clinical results. 15th International Conference on Cochlear Implants. 2018:351-352.

60. Caversaccio M, Wimmer W, Anso J, Mantokoudis G, Gerber N, Rathgeb C, Schneider D, Hermann J, Wagner F, Scheidegger O. Robotic middle ear access for cochlear implantation: first in man. PloS one. 2019;14(8):e0220543.

61. Rau TS, Kreul D, Lexow J, Hugl S, Zuniga MG, Lenarz T, et al. Characterizing the size of the target region for atraumatic opening of the cochlea through the facial recess. Comput Med Imaging Graph. 2019;77:101655.

62. Schneider D, Stenin I, Ansó J, Hermann J, Mueller F, Pereira Bom Braga G, et al. Robotic cochlear implantation: feasibility of a multiport approach in an ex vivo model. Eur Arch Otorhinolaryngol. 2019;276(5):1283-1289.

63. Braga GOTB, Schneider D, Muller F, Hermann J, Weber S, Caversaccio M. Feasibility of pediatric robotic cochlear implantation in phantoms. Otol Neurotol. 2020;41(2):e192-e200.

64. Riojas KE, Labadie RF. Robotic Ear Surgery. Otolaryngol Clin North Am. 2020;53(6):1065-1075.

65. Mueller F, Hermann J, Weber S, Braga GOTB, Topsakal V. Image-based planning of minimally traumatic inner ear access for robotic cochlear implantation. Front Surg. 2021;8.

66. Ansó J, Scheidegger O, Wimmer W, Gavaghan K, Gerber N, Schneider D, et al. Neuromonitoring during robotic cochlear implantation: initial clinical experience. Ann Biomed Eng. 2018;46:1568-1581.

67. Vittoria S, Lahlou G, Torres R, Daoudi H, Mosnier I, Mazalaigue S, et al. Robot-based assistance in middle ear surgery and cochlear implantation: first clinical report. Eur Arch Otorhinolaryngol. 2021;278:77-85.

68. Kaufmann CR, Henslee AM, Claussen A, Hansen MR. Evaluation of insertion forces and cochlea trauma following robotics-assisted cochlear implant electrode array insertion. Otol Neurotol. 2020;41(5):631-638.

69. Pelliccia P, Venail F, Bonafé A, Makeieff M, Iannetti G, Bartolomeo M, Mondain M. Cochlea size variability and implications in clinical practice. Acta Otorhinolaryngol Ital. 2014;34(1):42.

70. Franke-Trieger A, Jolly C, Darbinjan A, Zahnert T, Mürbe D. Insertion depth angles of cochlear implant arrays with varying length: a temporal bone study. Otol Neurotol. 2014;35(1):58-63.

71. Alexiades G, Dhanasingh A, Jolly C. Method to estimate the complete and two-turn cochlear duct length. Otol Neurotol. 2015;36(5):904-907.

72. Escude B, James C, Deguine O, Cochard N, Eter E, Fraysse B. The size of the cochlea and predictions of insertion depth angles for cochlear implant electrodes. Audiol Neurootol. 2006;11 Suppl 1:27-33.

73. Labadie RF, Balachandran R, Noble JH, Blachon GS, Mitchell JE, Reda FA, et al. Minimally invasive image-guided cochlear implantation surgery: first report of clinical implementation. Laryngoscope. 2014;124(8):1915-1922.

74. Hardy M. The length of the organ of Corti in man. Am J Anat. 1938;62(2):291-311.

75. Retzius G. Das Gehörorgan der Wirbelthiere: Morphologisch-histologische Studien. Das Gehörorgan der Reptilien, der Vögel und der Säugethiere. Gedruckt in der Centraldruckerei, 1884.

76. Koch RW, Ladak HM, Elfarnawany M, Agrawal SK. Measuring cochlear duct length–a historical analysis of methods and results. J Otolaryngol Head Neck Surg. 2017;46:1-11.

77. Jeffery N, Spoor F. Prenatal growth and development of the modern human labyrinth. J Anat 2004;204(2):71-92.

78. Dimopoulos P, Muren C. Anatomic variations of the cochlea and relations to other temporal bone structures. Acta Radiol. 1990;31(5):439-444.

79. Ketten DR, Skinner MW, Wang G, Vannier MW, Gates GA, Gail Neely J. In vivo measures of cochlear length and insertion depth of nucleus cochlear implant electrode arrays. Ann Otol Rhinol Laryngol Suppl. 1998;175.

80. Erixon E, Högstorp H, Wadin K, Rask-Andersen H. Variational anatomy of the human cochlea: implications for cochlear implantation. Otol Neurotol. 2009;30(1):14-22.

81. Meng J, Li S, Zhang F, Li Q, Qin Z. Cochlear size and shape variability and implications in cochlear implantation surgery. Otol Neurotol. 2016;37(9):1307-1313.

82. Úlehlová L, Voldřich L, Janisch R. Correlative study of sensory cell density and cochlear length in humans. Hear Res. 1987;28(2-3):149-151.

83. Bredberg G. Cellular pattern and nerve supply of the human organ of Corti. Acta Otolaryngol. 1968;236:1-135.

84. Wright A, Davis A, Bredberg G, Ulehlova L, Spencer H. Hair cell distributions in the normal human cochlea. Acta Otolaryngol Suppl. 1987;444:1-48.

85. Sridhar D, Stakhovskaya O, Leake PA. A frequency-position function for the human cochlear spiral ganglion. Audiol Neurootol. 2006;11(Suppl. 1):16-20.

86. Stakhovskaya O, Sridhar D, Bonham BH, Leake PA. Frequency map for the human cochlear spiral ganglion: implications for cochlear implants. J Assoc Res Otolaryngol. 2007;8:220-233.

87. Guild SR. A graphic reconstruction method for the study of the organ of Corti. Anat Rec. 1921;22:141-157.

88. Walby AP. Scala tympani measurement. Ann Otol Rhinol Laryngol. 1985;94(4):393-397.

89. Pollak A, Felix H, Schrott A. Methodological aspects of quantitative study of spiral ganglion cells. Acta Otolaryngol Suppl. 1987;104(sup436):37-42.

90. Lee J, Nadol Jr JB, Eddington DK. Depth of electrode insertion and postoperative performance in humans with cochlear implants: a histopathologic study. Audiol Neurootol. 2010;15(5):323-331.

91. Rivas A, Cakir A, Hunter JB, Labadie RF, Zuniga MG, Wanna GB, et al. Automatic cochlear duct length estimation for selection of cochlear implant electrode arrays. Otol Neurotol. 2017;38(3):339.

92. Wimmer W, Gerber N, Dhanasingh A, Mistrik P, Jolly C, Bell B, et al. In-vitro microCT validation of preoperative cochlear duct length estimation. CURAC. 2013;1477:143-146.

93. Shin KJ, Lee JY, Kim JN, Yoo JY, Shin C, Song WC, et al. Quantitative analysis of the cochlea using three-dimensional reconstruction based on microcomputed tomographic images. Anat Rec (Hoboken). 2013;296(7):1083-1088.

94. Verbist BM, Ferrarini L, Briaire JJ, Zarowski A, Admiraal-Behloul F, Olofsen H, et al. Anatomic Considerations of Cochlear Morphology and Its Implications for Insertion Trauma in Cochlear Implant Surgery. Otol Neurotol. 2009;30(4):471-477.

95. Sato H, Sando I, Takahashi H. Sexual dimorphism and development of the human cochlea: computer 3-D measurement. Acta Otolaryngol. 1991;111(6):1037-1040.

96. Würfel W, Lanfermann H, Lenarz T, Majdani O. Cochlear length determination using cone beam computed tomography in a clinical setting. Hear Res. 2014;316:65-72.

97. Skinner MW, Ketten DR, Holden LK, Harding GW, Smith PG, Gates GA, et al. CT-derived estimation of cochlear morphology and electrode array position in relation to word recognition in Nucleus-22 recipients. J Assoc Res Otolaryngol. 2002;3:332-350.

98. Takagi A, Sando I. Computer-aided three-dimensional reconstruction: a method of measuring temporal bone structures including the length of the cochlea. Ann Otol Rhinol Laryngol. 1989;98(7):515-522.

99. Kawano A, Seldon HL, Clark GM. Computer-aided three-dimensional reconstruction in human cochlear maps: measurement of the lengths of organ of Corti, outer wall, inner wall, and Rosenthal's canal. Ann Otol Rhinol Laryngol. 1996;105(9):701-709.

100. Chen JL, Gittleman A, Barnes PD, Chang KW. Utility of temporal bone computed tomographic measurements in the evaluation of inner ear malformations. Arch Otolaryngol Head Neck Surg. 2008;134(1):50-56.

101. Grover M, Sharma S, Singh SN, Kataria T, Lakhawat RS, Sharma MP. Measuring cochlear duct length in Asian population: worth giving a thought! Eur Arch Otorhinolaryngol. 2018;275(3):725-728.

102. Iyaniwura JE, Elfarnawany M, Riyahi-Alam S, Sharma M, Kassam Z, Bureau Y, Parnes LS, Ladak HM, Agrawal SK. Intra-and interobserver variability of cochlear length measurements in clinical CT. Otol Neurotol. 2017;38(6):828-832.

103. Lan M-Y, Shiao J-Y, Ho C-Y, Hung H-C. Measurements of normal inner ear on computed tomography in children with congenital sensorineural hearing loss. Eur Arch Otorhinolaryngol. 2009;266:1361-1364.

104. OTOPLAN - Patient specific otological planning sofware, https://www.cascination.com/en/otoplan, Accessing date: 16.08.2023.

105. Zahara D, Dewi RD, Aboet A, Putranto FM, Lubis ND, Ashar T. Variations in cochlear size of cochlear implant candidates. Int Arch Otorhinolaryngol. 2019;23:184-190.

106. van der Marel KS, Briaire JJ, Wolterbeek R, Snel-Bongers J, Verbist BM, Frijns JH. Diversity in cochlear morphology and its influence on cochlear implant electrode position. Ear Hear. 2014;35(1):e9-e20.

107. Rask-Andersen H, Erixon E, Kinnefors A, Löwenheim H, Schrott-Fischer A, Liu W. Anatomy of the human cochlea–implications for cochlear implantation. Cochlear Implants Int. 2011;12(sup1):S13-S18.

108. Lloyd SK, Kasbekar AV, Kenway B, Prevost T, Hockman M, Beale T, et al. Developmental changes in cochlear orientation-implications for cochlear implantation. Otol Neurotol. 2010;31(6):902-907.

109. Tange R. Modifications on the Alternative Method for Cochlea Implantation.İçinde: Umad C, Antony Tange R (Editörler). Cochlear Implant Research Updates. 2012: s.23-32.

110. Bruijnzeel H, Ziylan F, Cattani G, Grolman W, Topsakal V. Retrospective complication rate comparison between surgical techniques in paediatric cochlear implantation. Clin Otolaryngol. 2016;41(6):666-672.

111. Öztürk K, Sercan G, Çelik S, Orhan M, Bilge O, Bilgen C, et al. Revisiting the anatomy of the facial recess: the boundaries of the round window exposure. Balkan Med J. 2016;33(5):552-555.

112. Bettman RH, Appelman AM, van Olphen AF, Zonneveld FW, Huizing EH. Cochlear orientation and dimensions of the facial recess in cochlear implantation. ORL J Otorhinolaryngol Relat Spec. 2003;65(6):353-358.

113. Wang L, Yang J, Jiang C, Zhang D. Cochlear implantation surgery in patients with narrow facial recess. Acta Otolaryngol. 2013;133(9):935-938.

114. Gudis DA, Montes M, Bigelow DC, Ruckenstein MJ. The round window: is it the "cochleostomy" of choice? Experience in 130 consecutive cochlear implants. Otol Neurotol. 2012;33(9):1497-1501.

115. Todt I, Basta D, Ernst A. Does the surgical approach in cochlear implantation influence the occurrence of postoperative vertigo? Otolaryngol Head Neck Surg. 2008;138(1):8-12.

116. Su WY, Marion MS, Hinojosa R, Matz GJ. Anatomical measurements of the cochlear aqueduct, round window membrane, round window niche, and facial recess. Laryngoscope. 1982;92(5):483-486.

117. Bielamowicz SA, Coker NJ, Jenkins HA, Igarashi M. Surgical dimensions of the facial recess in adults and children. Arch Otolaryngol Head Neck Surg. 1988;114(5):534-537.

118. Young Y-S, Nadol Jr JB. Dimensions of the extended facial recess. Ann Otol Rhinol Laryngol. 1989;98(5):336-338.

119. Eby TL. Development of the facial recess: implications for cochlear implantation. Laryngoscope. 1996;106(S80):1-7.

120. Jain S, Deshmukh P, Lakhotia P, Kalambe S, Chandravanshi D, Khatri M. Anatomical study of the facial recess with implications in round window visibility for cochlear implantation: personal observations and review of the literature. Int Arch Otorhinolaryngol. 2019;23:281-291.

121. Copson B, Wijewickrema S, Ma X, Zhou Y, Gerard JM, O'Leary S. Surgical approach to the facial recess influences the acceptable trajectory of cochlear implantation electrodes. Eur Arch Otorhinolaryngol. 2022;279(1):137-147.

122. Zhu Y, Tong B, Xu S, Liu Y, Duan M. Applied anatomy of operation through posterior tympanum approach. Lin Chuang Er Bi Yan Hou Tou Jing Wai Ke Za Zhi. 2008;22(19):867-870.

123. Calli C, Pinar E, Oncel S, Tatar B, Tuncbilek MA. Measurements of the facial recess anatomy: implications for sparing the facial nerve and chorda tympani during posterior tympanotomy. Ear Nose Throat J. 2010;89(10).

124. Maru N, Cheita A, Mogoanta CA, Prejoianu B. Intratemporal course of the facial nerve: morphological, topographic and morphometric features. Rom J Morphol Embryol. 2010;51(2):243-248.

125. Jeon E-J, Jun B, Song J-N, Kim J-E, Lee DH, Chang K-H. Surgical and radiologic anatomy of a cochleostomy produced via posterior tympanotomy for cochlear implantation based on three-dimensional reconstructed temporal bone CT images. Surg Radiol Anat. 2013;35:471-475.

126. Diogo I, Walliczeck U, Taube J, Franke N, Teymoortash A, Werner J, et al. Possibility of differentiation of cochlear electrodes in radiological measurements of the intracochlear and chorda-facial angle position. Acta Otorhinolaryngol Ital. 2016;36(4):310.

127. Zou T, Xie N, Guo M, Shu F, Zhang H. Applied anatomy of facial recess and posterior tympanum related to cochlear implantation. Lin Chuang er bi yan hou tou Jing wai ke za zhi. 2012;26(10):445-448.

128. Wang H, Shan X, Meng Z, Sun H, Zhao L. Anatomical measurements and clinical applications through facial recess approach. Lin Chuang er bi yan hou tou Jing wai ke za zhi. 2013;27(13):708-711.

129. Kashio A, Sakamoto T, Karino S, Kakigi A, Iwasaki S, et al. Predicting round window niche visibility via the facial recess using high-resolution computed tomography. Otol Neurotol. 2015;36(1):e18-e23.

130. Wang L-E, Xia J, Shen X-X, Wang Z-X, Wang W, Zhang D-X. Retaining chorda tympani nerve integrity during cochlear implant surgery. Chin Med J (Engl). 2015;128(15):2115-2118.

131. Dai P, Zhang T, Wang K, Song J, Qian W, Wang Z. Positional relationship between the facial nerve and other structures of the temporal bone. J Laryngol Otol. 2004;118(2):106-111.

132. Scarpa A. Antonii Scarpa... De structura fenestrae rotundae auris, et de tympano secundario anatomicae observationes. Societas typographica, 1772.

133. Bonaldi LV, De Angelis M, Smith RL. Developmental study of the round window region. Acta Anat (Basel). 1997;159(1):25-29.

134. Meshik X, Holden TA, Chole RA, Hullar TE. Optimal cochlear implant insertion vectors. Otol Neurotol. 2010;31(1):58.

135. Takahashi H, Takagi A, Sando I. Computer-aided three-dimensional reconstruction and measurement of the round window and its membrane. Otolaryngol Head Neck Surg. 1989;101(5):517-521.

136. Cohen D, Blinder G, Perez R, Raveh D. Standardized computed tomographic imaging and dimensions of the round-window niche. Int Tinnitus J. 2005;11(2):158.

137. Singla A, Sahni D, Gupta A, Loukas M, Aggarwal A. Surgical anatomy of round window and its implications for cochlear implantation. Clin Anat. 2014;27(3):331-336.

138. Seliet AM, El Hamshary AS, El Refai AM, Ali AM, Gabal SR. Human round window: morphometry and topographical anatomy and their effect on cochlear implantation. BMFJ. 2018;35(2):246.

139. Chen K, Lyu H, Xie Y, Yang L, Zhang T, Dai P. Morphological characteristics of round window niche in congenital aural atresia and stenosis patients. J Comput Assist Tomogr. 2015;39(4):547-551.

140. Stewart T, Belal A. Surgical anatomy and pathology of the round window. Clin Otolaryngol Allied Sci. 1981;6(1):45-62.

141. ten Donkelaar HJ, Elliott KL, Fritzsch B, Kachlik D, Carlson M, Isaacson B, et al. An updated terminology for the internal ear with combined anatomical and clinical terms. J Phonet Audiol. 2020;6(10.35248):2471-9455.2420.

142. Takahashi H, Sando I, Takagi A. Computer-aided three-dimensional reconstruction and measurement of the round window niche. Laryngoscope. 1989;99(5):505-509.

143. Torres R, Drouillard M, De Seta D, Bensimon J-L, Ferrary E, Sterkers O, et al. Cochlear implant insertion axis into the basal turn: a critical factor in electrode array translocation. Otol Neurotol. 2018;39(2):168-176.

144. Daoudi H, Lahlou G, Torres R, Sterkers O, Lefeuvre V, Ferrary E, et al. Robot-assisted cochlear implant electrode array insertion in adults: a comparative study with manual insertion. Otol Neurotol. 2021;42(4):e438-e444.

145. Johnston JD, Scoffings D, Chung M, Baguley D, Donnelly NP, Axon PR, et al. Computed tomography estimation of cochlear duct length can predict full insertion in cochlear implantation. Otol Neurotol. 2016;37(3):223-228.

146. Salcher R, Boruchov A, Timm M, Steffens M, Giesemann A, Lenarz T, et al. On the Intracochlear Location of Straight Electrode Arrays After Cochlear Implantation: How Lateral Are Lateral Wall Electrodes? Otol Neurotol. 2021;42(2):242-250.

147. Hochmair I, Arnold W, Nopp P, Jolly C, Müller J, Roland P. Deep Electrode Insertion in Cochlear Implants: Apical Mrphology, Electrodes and Speech Perception Results. Acta Otolaryngol. 2003;123(5):612-617.

148. Wanna GB, Noble JH, Gifford RH, Dietrich MS, Sweeney AD, Zhang D, et al. Impact of intrascalar electrode location, electrode type, and angular insertion depth on residual hearing in cochlear implant patients: preliminary results. Otol Neurotol. 2015;36(8):1343.

149. Roy AT, Penninger RT, Pearl MS, Wuerfel W, Jiradejvong P, Carver C, et al. Deeper cochlear implant electrode insertion angle improves detection of musical sound quality deterioration related to bass frequency removal. Otol Neurotol. 2016;37(2):146-151.

150. O'Connell BP, Cakir A, Hunter JB, Francis DO, Noble JH, Labadie RF, et al. Electrode location and angular insertion depth are predictors of audiologic outcomes in cochlear implantation. Otol Neurotol. 2016;37(8):1016.

151. Postelmans J. Cochlear implantation: Surgical and audiological assessment of cochlear implantation techniques. Maastricht2012: s.53-60.

152. Tange RA, Topsakal V, Smulders YE, Grolman W. Mastoid cavity after cochlear implant surgery with the mastoid saving surgical approach method. Int Adv Otol. 2010;6:29-33.

8. APPENDICES

8.1. Ethical approval

Universitair Ziekenhuis Brussel

VRIJE UNIVERSITEIT BRUSSEL

VEDAT TOPSAKAL
NKO

Brussels, 2022-09-27

EC number: **EC-2022-257**

MEDICAL ETHICS COMMITTEE - OPINION

Concerning :
Investigation of cochlea dimensions in patients who had undergone robotic and conventional cochlear implantation surgery
BUN: 1432022000187

During the meeting of 2022-09-14, the Medical Ethics Committee of UZ Brussel/VUB reviewed and approved the above mentioned project from the ethical, legal and medical science points of view.

Upon receipt of the adapted documents (see annex EC document list), the Ethics Committee decides that there are no objections to the study in its present form.

Please remark that the Green Light Procedure has to be completed.

This approval is valid for the duration of the trial. The Committee wishes to obtain an annual trial status. Results of the trial should be transmitted to the Committee at the end of the trial (publication or summary if there is no publication planned). The Committee reminds the investigator of his/her personal responsibility for this project. The Committee does not take any responsibility for its favourable advice of the project. The Ethics Committee is organised and operates according to ICH-GCP and its applicable laws and regulations. The list of members is enclosed.

Kind regards,

Chairman
Vice-Chairman

9. CURRICULUM VITAE

. She has completed undergraduate education at Gaziantep University Faculty of Health Sciences, Department of Physical Therapy and Rehabilitation between 2012-2016. In 2019, she completed master degree at Gaziantep University Institute of Health Sciences Anatomy Department and started her doctorate education in the same department. Since 2022, she has been working as a Research Assistant in Gaziantep University Faculty of Medicine,
Anatomy and continues her Ph.D. education.